UNIVERSITY OF LJUBLJANA

Faculty of Mechanical Engineering

Analiza mehanskih obremenitev in primerjava rešitev za enosmerne sklopke za pogone električnih koles

Mechanical load analysis and benchmarking of one-way clutches for e-bike drives

A Master's thesis of the second-cycle master's study programme in MECHANICAL ENGINEERING – a research and development programme

Enric Viñals Domènech

Ljubljana, June 2018

UNIVERSITY OF LJUBLJANA

Faculty of Mechanical Engineering

Analiza mehanskih obremenitev in primerjava rešitev za enosmerne sklopke za pogone električnih koles

Mechanical load analysis and benchmarking of one-way clutches for e-bike drives

A Master's thesis of the second-cycle master's study programme in MECHANICAL ENGINEERING – a research and development programme

Enric Viñals Domènech

Advisor: prof. dr. Jože Tavčar
Co-advisor: assist. prof. dr. Samo Zupan

Ljubljana, June 2018

Acknowledgements

I would like to thank all the people that have been involved in this project, gave me support and assisted me at any point to fulfil my goal.

First, I would like to thank my mentor, assoc. prof. dr. Jože Tavčar, for his support and advice during the development of this project, and also for having his office door open when I had any doubts or questions on how to proceed.

I would like to thank also assist. prof. dr. Samo Zupan, who gave me a new perspective of the project, and made recommendations on how the project could be improved.

To the people working in LECAD, where I have been developing the master thesis, for being so kind and helping me whenever I needed.

And last but not least, to my family, who have been a great support during all these years and not letting me down when I was lost. And also to all the friends that have been suffering me and still have supported me during a long time.

Declaration

I, the undersigned Enric Vinals Domenech, student from Erasmus Exchange on the Faculty Of Mechanical Engineering at the University of Ljubljana, with registration number 70080970, author of the written final work of studies, entitled: Mechanical load analysis and benchmarking of one-way clutches for e-bike drives,

DECLARE that

1. The written final work of studies is a result of my independent work;
2. The printed form of the written final work of studies is identical to the electronic form of the written final work of studies;
3. I acquired all the necessary permissions for the use of data and copyrighted works in the written final work of studies and clearly marked them in the written final work of studies;
4. During the preparation of the written final work of studies I acted in accordance with ethical principles and obtained, where necessary, agreement of the ethics commission;
5. I give my consent to the use of the electronic form of the written final work of studies for the detection of content similarity with other works, using similarity detection software that is connected with the study information system of the university member;
6. I transfer to the UL – free of charge, non-exclusively, geographically and time-wise unlimited – the right of saving the work in the electronic form, the right of reproduction, as well as the right of making the written final work of studies available to the public on the World Wide Web via the Repository of the UL;
7. I give my consent to the publication of my personal data included in the written final work of studies and in this declaration, together with the publication of the written final work of studies;
8. I give my consent to the use of my birth date in COBISS record.

In Ljubljana, _____ Student's signature: _____

Abstract

UDC 004.942:519.876.5:621.825(043.2)

Serial No.: MAG II/519 E

Mechanical load analysis and benchmarking of one-way clutches for e-bike drives

Enric Viñals Domènech

Keywords: One-way clutch
Numerical simulation
Electric bike drive
Ratchet and pawl clutch
Sprag clutch

An overview of one-way clutches, used design principles and criteria for selection was prepared. The main problem while designing an e-bike drive using a sprag clutch was the assembly tolerances. Therefore, an analysis using the finite element method of two different type of clutches was conducted. In order to do these analyses, 3D model of sprag clutch and the ratchet and pawl clutch have been created. For each clutch type the calculations of the loads have been made, and used them to run the simulations. Once the simulations have been done, the deformation and the von Mises stress values have been checked to verify if the designs could bear the loads applied. After verifying the models, the materials, which the clutches should be made in order to bear the applied loads, are proposed. On the base of multiple criteria assessment ratchet and pawl clutch was selected as more appropriate.

Povzetek

UDC 004.942:519.876.5:621.825(043.2)

Tek. štev.: MAG II/519 E

Analiza mehanskih obremenitev in primerjava rešitev za enosmerne sklopke za pogone električnih koles

Enric Viñals Domènech

Ključne besed: enosmerna sklopka
numerična simulacija
pogon električnega kolesa
oblikovna sklopka
torna sklopka

Pripravljen je bil pregled enosmernih sklopk, uporabljenih principov delovanja in postavljeni so bili kriteriji za izbiro. Glavna težava pri načrtovanju pogona e-koles z uporabo torne sklopke so bili dovoljeni odstopki sestava. Zato je bila opravljena analiza z uporabo metod končnih elementov dveh različnih tipov sklopk. Da bi naredili te analize, so bili izdelani 3D modeli za torno in oblikovno sklopko. Za vsako vrsto sklopke je bil postavljen model obremenitev in robnih pogojev ter v naslednjem koraku je bila izvedena numerična simulacija. Na osnovi rezultatov simulacije, so bile preverjene deformacije in vrednosti primerjalnih napetosti pri predvidenih obremenitvah. Po preverjanju modelov so predlagani materiali, ki jih je treba uporabiti za prenos predvidenih obremenitev. Na podlagi več kraterijev je bila kot primernejša izbrana oblikovna sklopka.

Table of contents

List of figures ..... **xv**
List of tables ..... **xvii**
List of symbols used ..... **xix**
List of acronyms used ..... **xxi**

1. Introduction **1**
1.1 Background **1**
1.2 Objectives **3**

2 Theoretical background and overall of literature **5**
2.1 Different applications of one-way clutches **5**
2.1.1 Overrunning 5
2.1.2 Indexing 6
2.1.3 Backstopping 6
2.2 Different types of one-way clutches **6**
2.2.1 The ratchet and pawl clutch 6
2.2.2 The spring clutch 7
2.2.3 The roller clutch 8
2.2.4 The sprag clutch 9
2.2.5 Summary of one-way clutches 10
2.3 Main differences between sprag clutches suppliers **12**
2.3.1 GMN 12
2.3.2 Ringspann 13
2.3.3 Cross Morse 15
2.3.4 Stieber 16
2.3.5 Tsubaki 17
2.3.6 Renold 18
2.4 Description of the clutches used in the e-bike drive **19**
2.4.1 GMN sprag clutch 20
2.4.2 Ratchet and pawl clutch 20

3 Methodology **23**
3.1 Sprag clutch simulations **23**
3.1.1 Simple cage simulation 28

3.1.2 Double-cage simulation 29
3.1.3 Alternative solutions 31
3.2 Ratchet and pawl simulations 33
3.2.1 Outer part simulation 35
3.2.2 Inner part simulation 35

4 Results and discussion 39

4.1 Sprag clutch results 39
4.1.1 Simple cage results 39
4.1.2 Double-cage results 41
4.1.3 Alternative results 52
4.2 Ratchet and pawl clutch results 53
4.2.1 Outer part results 53
4.2.2 Inner part results 55
4.2.3 Complete part results 59
4.3 Comparison between the sprag and the ratchet and pawl clutch 66

5 Conclusions 69

6 Bibliography 71

List of figures

Figure 1.1: Image of the FE 448 Z2 [1] and the FE 453 M [2] clutches. 1
Figure 1.2: Ratchet and pawl clutch used in the first prototypes. 2
Figure 2.1: Ratchet and pawl clutch [5]. 7
Figure 2.2: Spring clutch [4]. 7
Figure 2.3: M-series schematic [7]. 8
Figure 2.4: Roller clutch [8]. 9
Figure 2.5: Sprag clutch [9]. 9
Figure 2.6: Driving torque vs. Freewheeling speed for the one-way clutches. 11
Figure 2.7: Decision tree for clutches. 12
Figure 2.8: (a) Z-type spring (b) Meander spring [12]. 13
Figure 2.9: (a) Sprag lift-off X in freewheeling operation, (b) Sprag lift-off X ready to be locked [8]. 14
Figure 2.10: (a) Sprag lift-off Z in freewheeling operation, (b) Sprag lift-off Z ready to be locked [8]. 14
Figure 2.11: (a) Hydrodynamic sprag lift-off in freewheeling operation, (b) Detail of the direction of oil pumping [8]. 15
Figure 2.12: Detail of the DC design by Stieber [5]. 16
Figure 2.13: Detail of the RSCI design by Stieber. (a) Torque transmission (b) Overrunning operation [5]. 17
Figure 2.14: Tsubaki CAM clutch [13]. 17
Figure 2.15: (a) Entire CAM Clutch is stationary (b) Inner race only turning (c) Inner and outer race locked and turning [13]. 18
Figure 2.16: Detail of the shapes of standard and ARO sprag clutch shape [14]. 19
Figure 2.17: ARO clutches conditions: (a) Normal conditions (b) extreme overload [14]. 19
Figure 2.18: Comparison between actual and 3-D model sprag. 20
Figure 2.19: Components of the ratchet and pawl clutch. 21
Figure 3.1: Forces and torque scheme. 24
Figure 3.2: Application of the F_N in the worst-case scenario. 25
Figure 3.3: Geometric analysis of the sprag. 26
Figure 3.4: Sketch of the relation between tangential and normal force. [17] 27
Figure 3.5: Sketch of the clutch used in the first set of simulations. 28
Figure 3.6: Boundary conditions and loads applied in the worst-case scenario. 29
Figure 3.7: Sketch of the inner cage. 30
Figure 3.8: Sketch of the outer cage. 30
Figure 3.9: Boundary conditions and loads applied to double-cage simulations. 31
Figure 3.10: Sketch of the design with a tighter wall. 32
Figure 3.11: Sketch of the design with the inclined wall. 32
Figure 3.12: Sketch of the ratchet and pawl clutch loads. 34
Figure 3.13: Boundary conditions and loads applied on the three-pawl simulation. 35

Figure 3.14: Sketch of the inner part of the cage. 36
Figure 3.15: Boundary conditions and loads applied at the three-pawl simulation..... 36
Figure 3.16: Boundary conditions and load applied for the hammer simulation. 37
Figure 3.17: Sketch of the hammer. 37
Figure 4.1: Maximum deformation on worst-case scenario for case 4. 40
Figure 4.2: Maximum deformation on best-case scenario for case 4. 40
Figure 4.3: Comparison between the deformations of the cases studied..... 41
Figure 4.4: Bonded contact simulation results. 43
Figure 4.5: Section of the total deformation in case 2. 44
Figure 4.6: Section of the total deformation in case 11. 44
Figure 4.7: Section of the deformation in case 17. 45
Figure 4.8: Section of the deformation in case 16. 45
Figure 4.9: Section of the deformation in case 13. 46
Figure 4.10: Frictional contact simulation results. 46
Figure 4.11: Inner surface (left) and sprag surface (right) for the deformation simulation. 48
Figure 4.12: Equivalent stress value for non-refined case 31. 50
Figure 4.13: Equivalent stress values for refined case 31. 50
Figure 4.14: Equivalent stress values for non-refined case 32. 51
Figure 4.15: Equivalent stress values for refined case 32. 51
Figure 4.16: Sketch of the second design with the tightened wall. 52
Figure 4.17: Maximum equivalent stress for the 3-pawl simulation. 53
Figure 4.18: Maximum equivalent stress for the 6-pawl simulation. 54
Figure 4.19: Equivalent stress values of the refined 6-pawl simulation. 55
Figure 4.20: Equivalent stress for the 3-pawl complete inner part simulation. 56
Figure 4.21: Equivalent stress for the 3-pawl hammer simulation. 56
Figure 4.22: Equivalent stress for the 6-pawl complete inner part simulation. 57
Figure 4.23: Equivalent stress for the 6-pawl hammer simulation. 57
Figure 4.24: Equivalent stress values of the refined 6-pawls clutch. 58
Figure 4.25: Equivalent stress values of the refined 6-pawls hammer simulation. 59
Figure 4.26: Contact connection on the complete. 60
Figure 4.27: Deformation on the X-axis of the hammer. 61
Figure 4.28: Deformation on the Y-axis of the hammer. 61
Figure 4.29: Total deformation distribution of the hammer. 62
Figure 4.30: Von Mises stress concentration for the hammer part. 62
Figure 4.31: Von Mises stress concentration for the inner part. 63
Figure 4.32: Deformation on the X-axis of the outer part. 64
Figure 4.33: Deformation on the Y-axis of outer part. 64
Figure 4.34: Total deformation distribution of the outer part. 65
Figure 4.35: Von Mises stress concentration for the outer part. 65

List of tables

Table 1.1: Comparison between the characteristics of the clutches used. 2
Table 2.1 Characteristics of FE 453 M. 20
Table 2.2: Ratchet and pawl material properties 21
Table 3.1: Geometry characteristics of the study cases. 31
Table 4.1: Deformation values for the simple cage simulations. 39
Table 4.2: Deformation values of the double-cage simulations with bonded contact. 42
Table 4.3: Deformation values of the double-cage simulations with frictional contact. 43
Table 4.4: Deformation values for the second set of simulations. 47
Table 4.5: Deformation values for the third set of simulations. 47
Table 4.6: Deformation values of the inner surface and the sprag surface. 48
Table 4.7: Deformation values of the mesh refined designs. 49
Table 4.8: Stress values for cases 31 and 32. 49
Table 4.9: Deformation values of the alternative simulations. 52
Table 4.10: Deformation and stress values of the outer cage simulation. 53
Table 4.11: Deformation and stress values for the refined outer 6-pawls simulation. 54
Table 4.12: Deformation and stress values of the inner part simulations. 55
Table 4.13: Deformation and stress values for the refined inner 6-pawls simulation. 58
Table 4.14: Maximum deformation and equivalent stress on the complete simulation. 60
Table 4.15: Main characteristics of the clutches studied. 67
Table 4.16: Materials chosen for each clutch part 67

List of symbols used

Symbol	Unit	Meaning
A	mm^2	Area of the sprag
a	mm	Gap
D	mm	Outer diameter
D_{ext}	mm	Outer diameter of the clutch
D_{int}	mm	Inner diameter of the clutch
d	mm	Inner diameter
F_C	N	Centrifugal force
F_F	N	Spring force
F_N	N	Normal force
F_t	N	Tangential force
L	mm	Length of the wall
M	Nm	Torque
m	kg	Mass
n_{max}	min^{-1}	Maximum angular velocity
n_p	/	Number of sprags
p	MPa	Sprag's pressure
S	/	Centre of gravity
s	mm	Distance
T_{nom}	Nm	Nominal torque
W	mm	Width
α'	rad	Permitted angle
α_i	rad	Inner strut angle
α_o	rad	Outer strut angle
μ	/	Friction coefficient

List of acronyms used

Acronym	Meaning
FEM	Finite element method

1. Introduction

1.1 Background

While the Laboratory of Engineering Design (LECAD) and Domel enterprise were developing together an e-drive for electric bicycle, several problems with the one-way clutches that were used appeared.

Firstly, it has to be said that two one-way clutches are used in the e-drive that was being developed. One of this clutches is used the same way as the clutches that are used in standard bicycles. They are used in order to let the cyclist stop his pedalling and let the bike keep its inertial movement. The second one-way clutch is used when the assisted pedalling is not working, because it has been shut down, the cyclist is not pedalling or the bicycle speed is over 25 km/h (in this case the pedalling assist stops working because of legislation regularities). Having this second one-way clutch reduces the pedalling force the cyclist has to do because he or she will not have to transmit the force through the gears. The problems appeared in this last case.

In the first prototypes, a GMN sprag clutch were used for the e-drive. The two clutches used were the FE 453 M for the pedal, and the FE 448 Z2 for the motor clutch. In Figure 1.1, an image of the both GMN clutches can be seen.

Figure 1.1: Image of the FE 448 Z2 [1] and the FE 453 M [2] clutches.

In order to test this e-drive, in total four different clutches were used in the prototypes. Three of those clutches were sprag clutches and the other one was a ratchet and pawl, both of those types are a specific kind of clutches that will be seen in more detail in the chapter 2.2.

For the motor clutch, the GMN FE 448 Z2 clutch mentioned before and a SUMA clutch were used. Both of freewheels have similar characteristics. Both clutches have the same dimensions; however, their mechanic characteristics are a bit different. In addition, their price is different; GMN's price was almost the double of SUMA's price. Most of the problems that could be seen with this clutches were due to assembly tolerances, and because sprag clutches work with friction, heavy forces appeared on the clutch, which made it to work in a bad way.

For the pedal clutch, the GMN 453 M clutch mentioned before and a ratchet and pawl were used. The ratchet and pawl clutch is like the one that appears in Figure 1.2. Its design is simpler than the sprag clutches. For the tests that have already been done, this kind of clutch has shown less problems than the sprag clutches. These fewer problems are due to the acceptance of higher tolerances compared to the sprag clutches.

Figure 1.2: Ratchet and pawl clutch used in the first prototypes.

In Table 1.1, the characteristics of the GMN and SUMA clutches can be seen. Despite the mechanical differences between both clutches, even when the torque and rotary speed were below the limit of the SUMA, the SUMA clutch did not work well, leading to a locking of the mechanism.

Table 1.1: Comparison between the characteristics of the clutches used.

	Pedal clutch	Motor clutch	
Characteristics	FE 453 M (GMN)	FE 448 Z2 (GMN)	FE 448 Z2 (SUMA)
d [mm]	45	40	40
D [mm]	53	48	48
W [mm]	12	7	7

T_{nom} [Nm]	321	156	122
n_{max} [min^{-1}]	3400	5500	2500
m [kg]	0,0275	0,0228	-

1.2 Objectives

The main goal of this thesis is to understand the behaviour of freewheel under a certain load. Moreover, to understand how did one of the one-way clutches bear the loads and the other one could not do it. In addition, a comparison between the sprag and the ratchet and pawl clutch will be done. In order to understand the behaviour of the clutches a FEM analysis will be done. This finite element analysis will be done with the ANSYS software, because it is one of the most used software related to finite element analysis, and because LECAD has its license to run it.

In addition, some secondary objectives will be met to have a big picture of the one-way clutches world and to help people decide which one to use in future projects. These secondary objectives are mainly, doing a benchmarking of the different one-way clutches that can be found currently in the market. Once the benchmarking is done, it will be easier to fulfil the next objective.

This next objective is to create a guide to help future users of one-way clutches choose one of the different types of freewheels that are most used. This secondary task will be held describing the capable applications of every kind of one-way clutch.

2 Theoretical background and overall of literature

Clutches are mechanical devices used to engage and disengage the power transmission from a driver shaft to a driven shaft. In clutches, one shaft is usually attached to a motor; however, it can also be attached to any other power unit, while the driven shaft provides the output power for work. Particularly, one-way clutches transmit torque in one direction from the input to the output.

2.1 Different applications of one-way clutches

Unidirectional or one-way clutches have basically three different uses as it is determined by Bickford, 1968 [1], and it is also represented in several catalogues of different suppliers, as GMN, Ringspann or Tsubaki. The three different uses are overrunning, backstopping and indexing.

2.1.1 Overrunning

Overrunning clutches can transmit torque if they turn in one direction. Although, if the clutch turns in the opposite direction, it will work idle, therefore, no torque will be transmitted.

One typical example is found in a two-speed drive, where a geared and an electric motor are connected to a single driven shaft through an overrunning clutch. The machine can work with each motor at a time, and the clutch switches between two motors automatically. The clutch engages when the geared motor is driving at low speed, and when the electric motor is the one running, the clutch overruns.

Another example of overrunning clutches can be seen in power-assisted bicycles, the one-way clutch transmits to the chain the driving power form the motor. When the motor is not running, the clutch remains disengaged, however the clutch shaft is receiving the driving force form the chain. On the other hand, when the motor is running, the motor acts on the

clutch, causing it to engage. Consequently, the drive force is transmitted form the clutch shaft to the chain, being first transmitted to the sprocket wheel.

2.1.2 Indexing

This is one of the most used applications of freewheels. One-way clutches as an indexing mechanism are used in several fields as material feed mechanisms in seeding, textile and washing machines, and also in transmissions and many other applications. The indexing freewheel transmits a back and forth motion into a stepped rotation. This intermittent stepping motion can be used in light load applications and in heavy load applications.

2.1.3 Backstopping

One-way clutches are used also as backstops in order to prevent reverse rotations. Therefore, in backstopping applications rotation is allowed in one direction and blocked in the other direction. The most common areas of application for backstops are in safety devices for example in gear motors or belt conveyors. The backstop prevents reverse rotation once the motor is off or the power falls. Using this device can prevent damage on machinery or other expensive equipment.

2.2 Different types of one-way clutches

There exists different kind of freewheels, their difference recalls in their mechanism. Following there is a description of the most used freewheels nowadays. As it has been stated by Orthwein, 1986 [4], the most used one-way clutches are spring clutches, roller clutches and sprag clutches. In addition, the ratchet and pawl clutch will be seen, because it is the simplest of them all, and it was also used to create the first prototypes of the e-bike drive.

The focus will be in this kind of clutches, however, as years have gone by different business have developed their own system of clutches. A description of the main unidirectional clutches will be seen below.

2.2.1 The ratchet and pawl clutch

It is one of the simplest one-way clutch designs. As its name indicates, the design consists of using a single ratchet and a pawl. The pawl can be attached to the inner hub or either the outer hub, and it has a spring loaded which allows the pawl, when the clutch is in the freewheel position, to pivot out of the way of the ratchet, but it is forced into engagement in the torque transmitting direction. In Figure 2.1, an example of this clutch can be seen.

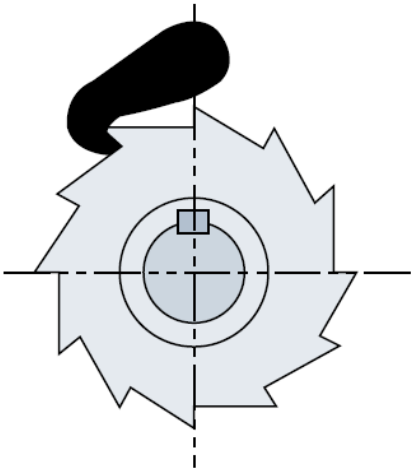

Figure 2.1: Ratchet and pawl clutch [5].

There are many possibilities for its design. Ratchet and pawl clutches can be designed with simple or multiple pawls. Moreover, in the case of the multiple pawls design two possibilities exists: one pawl at a time actuates or more than one pawl are meant to transmit the torque.

The main advantages of ratchet and pawl clutches are its simplicity and low cost. It is important to be remarked that this kind of clutch is not dependant on friction to work; it uses the shape of the teeth to work, which provides a high torque capacity with low spin loss.

2.2.2 The spring clutch

It consists of a helical spring wrapped around the input and the output hubs, but it is attached to neither of them. In Figure 2.2, a scheme of a simple spring clutch design can be seen. The first description of this clutch was done by Wiebusch, 1939 [6].

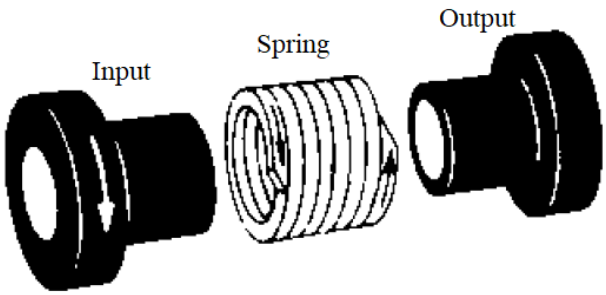

Figure 2.2: Spring clutch [4].

The working mechanism for this kind of clutches is that if the input driver rotates in one direction, the spring tightens and so the friction increases, this is how two shafts spin

together. However, if the rotation is in the other direction, the spring loosens, and then the spring produces a relatively small friction, which leads to the freewheeling.

Some of the advantages of using the spring clutch are that they have a simple construction and not many parts and they have a very fast engagement. Nevertheless, they have some inconvenient as they often wear out rapidly, and are not suited for high-speed applications.

Nowadays there are different types of spring clutches. For example, the supplier Tiny-Clutch has three different series of spring clutches. Two of those series (SP and M Series) are unidirectional; on the contrary, the AD-Series are a bidirectional freewheeling output.

The SP-Series consists of three parts, the same parts that appear on Figure 2.2, input hub, output hub and the spring. Its working mechanism is the same that has been explained before.

The M-series, on the other hand, has a different working mechanism. It uses an electromagnetic coil. When there is no power, the two hubs can rotate independently. When there is a magnetic force, it is used to wrap down the spring and couple the two hubs to transmit the torque. In Figure 2.3, the schematic of the M-series can be seen.

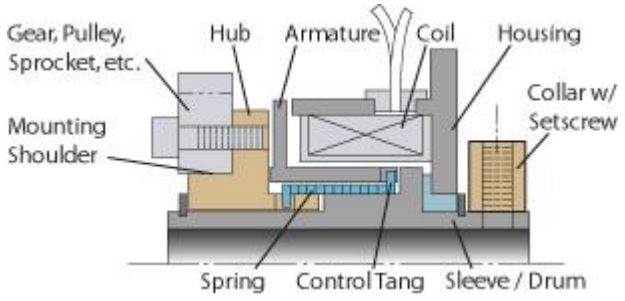

Figure 2.3: M-series schematic [7].

2.2.3 The roller clutch

Many configurations exist for roller clutches, as they can be used with balls, rollers or needles. Clutches made with needles are called needle roller clutch, and the greatest difference between needle roller and roller clutches is the diameter of the roller used, being much lower in the needles. Modern roller clutches are using a spring to keep the ball or the roller in contact with the inner and outer race.

The principle of operation of these clutches consists of balls that run between an outer and inner race. The profile of one of the races is designed so the balls can rotate freely in one of the directions, and transmit the torque in the other direction.

For the rolling clutch in the Figure 2.4, in order to it can be turned freely clockwise, the inner ring must be at a standstill, must be turned counter clockwise or must be turned clockwise but slower than the inner ring.

Some of the advantages of roller clutches are that they do not transmit torque until the input driver rotates faster than the output and their price, which is fairly cheap. However, these kind of clutches tend to have some friction and wear of issues.

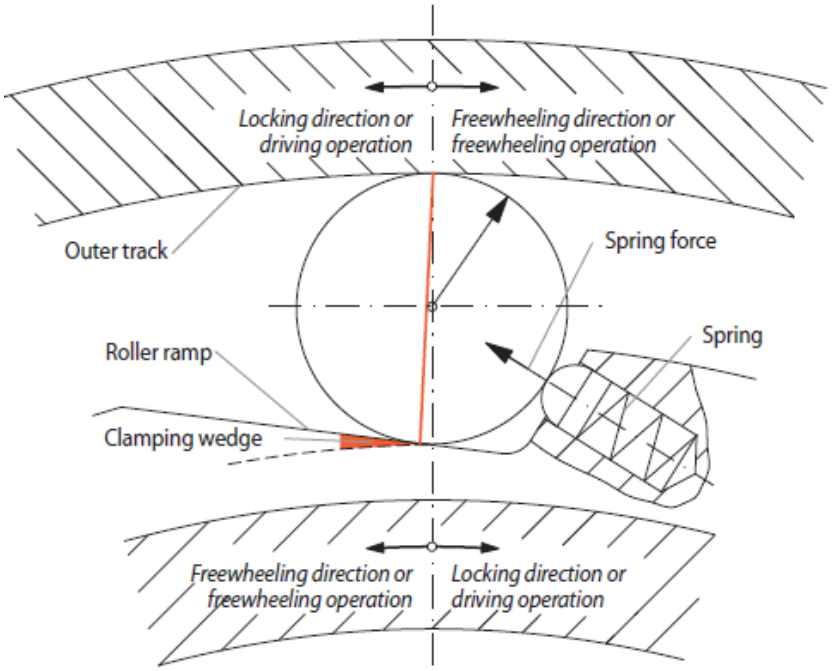

Figure 2.4: Roller clutch [8].

2.2.4 The sprag clutch

Sprag clutches are one of the most used clutches in required overrunning applications. Unlike rolling clutches, sprag clutches do not use balls or rollers between the inner and outer race, instead of these, sprag clutches incorporate a series of sprags, like little hammers, that are placed around the entire inner race. In Figure 2.5, the intern parts of a sprag clutch can be seen.

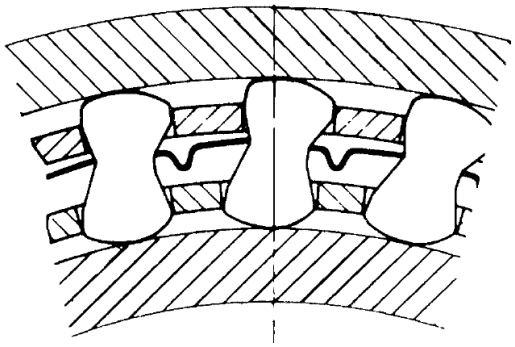

Figure 2.5: Sprag clutch [9].

Sprags are cylinders whose shape allows them to engage and disengage in a friction of a turn. They are designed to be thinner than balls or rollers, this way more sprags can fit in the given space, consequently, a greater torque can be transmitted. A spring is used in sprag clutches in order to ensure continuous friction contact between the sprags and the rings.

In order to get a good behaviour of sprag clutches it is important that the dimensions of the sprag, and the outer and the inner rings are designed correctly. Many studies have been carried out to determine the optimum parameters for the sprags, such as the Orthwein in 1986 [4], where the equations for determining the gripping angle were determined, or the model that Xu and Lowen presented on 1994 [10], that introduced a complete mathematical model for a sprag clutch.

The main advantage of sprag clutches is that they are able to transmit large torques than other one-way clutches of the same size dimension. This torque increase is given because more sprags than rollers can be located in each type of clutch. In addition, the increase of the radius curvature reduces the contact stress for a given force; in consequence, more force can be applied before getting to a critical stress contact point. Its main inconvenient is the higher cost compared to the other clutches, because of its geometry and the quantity of elements the clutch has, and also that they are quite sensitive on assembly tolerances.

2.2.5 Summary of one-way clutches

As it has been mentioned before in this chapter, different one-way clutches exist. In this subchapter a brief summary will be shown, this way it will be easier to compare the different clutches between them.

To summarize the values of torque transmission and freewheel velocity the Figure 2.6 can be seen. The graphic is based on the graph that published M. Neal on 1973 [11], but updating the values to nowadays clutches. The values of the driving torque for the sprag clutch go to approximately 950 kNm, and for the roller clutch near 175 kNm.

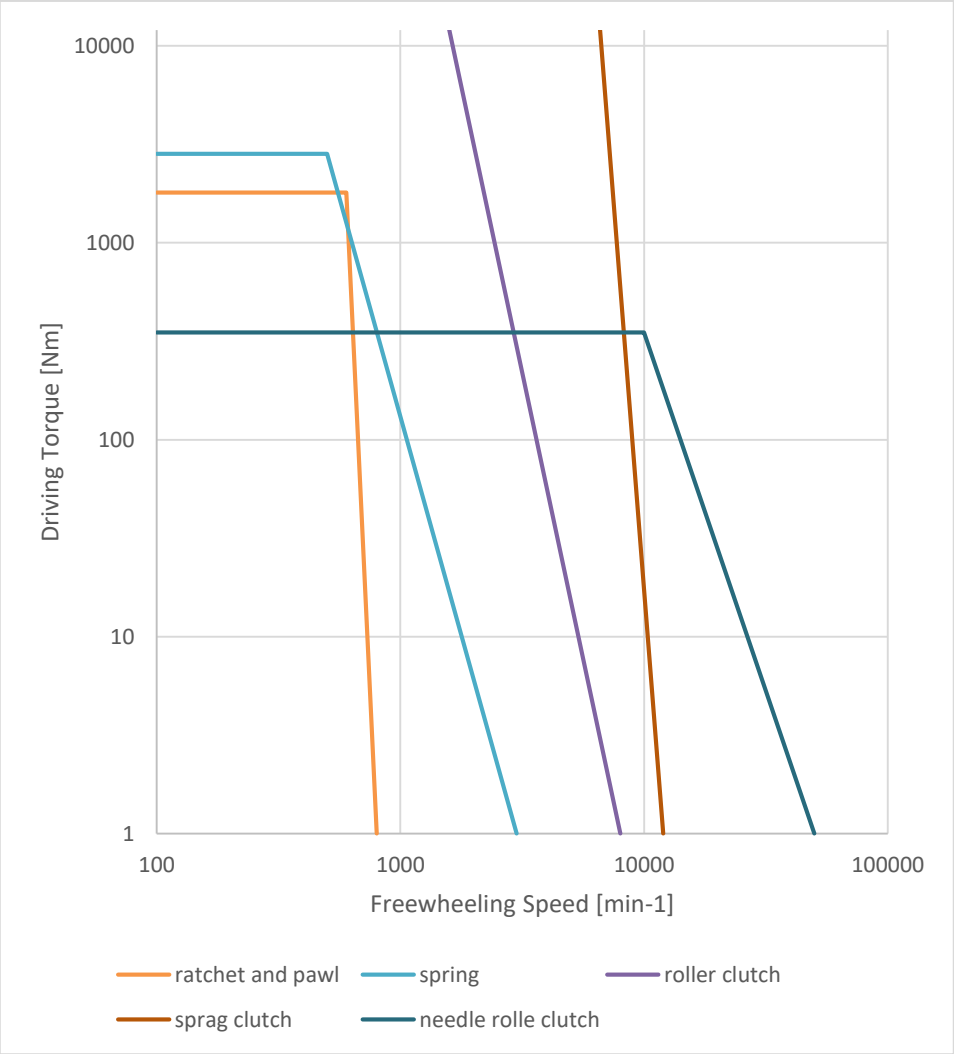

Figure 2.6: Driving torque vs. Freewheeling speed for the one-way clutches.

After collecting data from different supplier's catalogues and some books, a decision tree for choosing a freewheel can be done, the main characteristics of the decision tree are the torque transmission and the freewheel speed. The decision tree can be seen in Figure 2.7, and its main purpose is to help other engineers to choose between the different clutches.

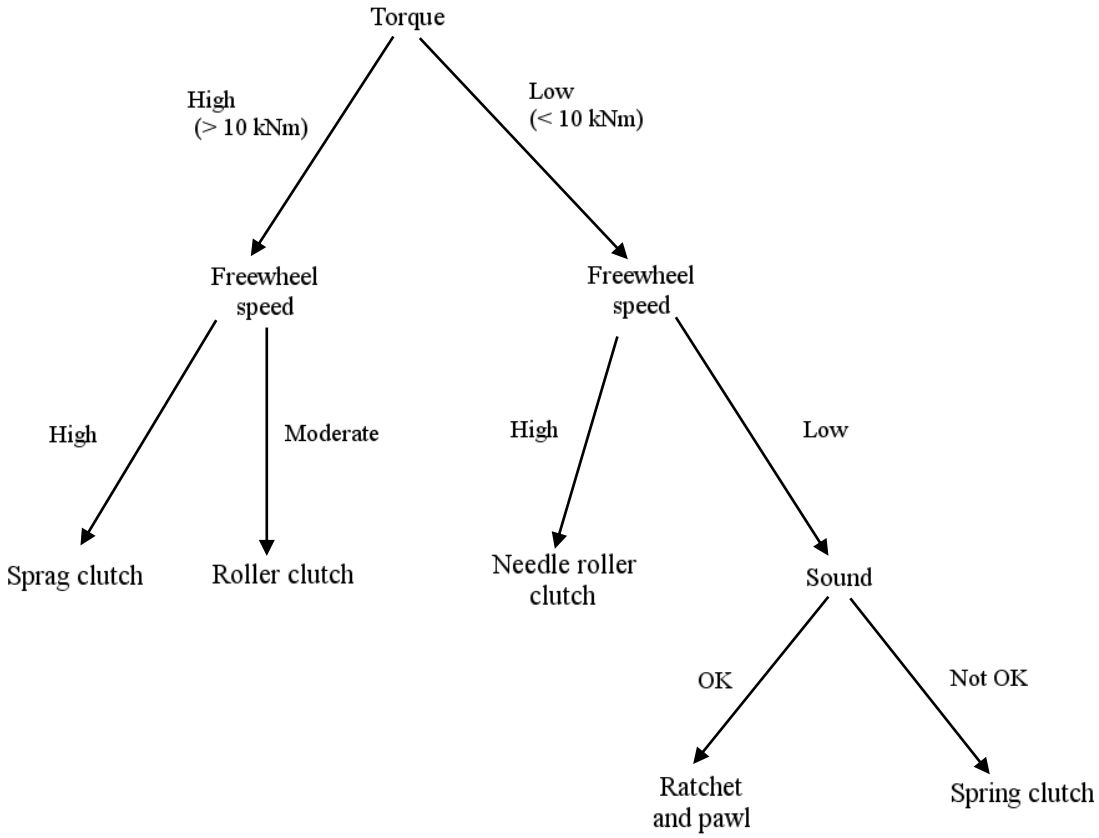

Figure 2.7: Decision tree for clutches.

2.3 Main differences between sprag clutches suppliers

There are, of course, different suppliers of sprag clutches, and they have some differences between their products. In this chapter, a brief description of the characteristics of some of the main suppliers of sprag clutches will be seen. The suppliers that will be seen here are GMN, Ringspann, Cross Morse, Stieber, Tsubaki and Renold.

2.3.1 GMN

In the sprag clutches from GMN two different methods of springs are used to maintain a constant friction between the sprags and the mating parts, as it has been said before. In Figure 2.8, the Z-type spring and the meander spring methods can be seen. The first method, which is the Z-type, consists on using a circular tension spring that envelope the sprags to maintain the friction. This method gives a longer life service in idle, but its transferable torque is inferior to the second method. This second method uses a special kind of spring, a 3-D

bended spring that actuates individually to each sprag, resulting in the increase of the torque transmitted. The meander spring is recommended for every precise and indexing applications, the Z-type, is suited for overrunning and backstopping applications.

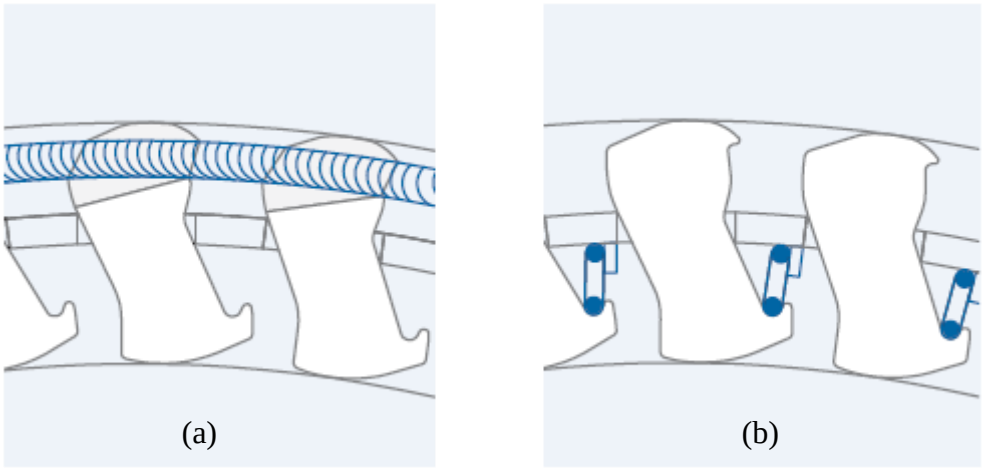

Figure 2.8: (a) Z-type spring (b) Meander spring [12].

2.3.2 Ringspann

Ringspann offers three special characteristics for overrunning clutches: with sprag lift-off X, with sprag lift-off Z and with hydrodynamic sprag lift-off.

The clutches with sprag lift-off X and Z are very similar. They are both used when the inner ring is rotating at high speed in freewheeling operations and the driving operation is done at low speed.

On Figure 2.9 and Figure 2.10, the F_C is the centrifugal force, F_F is the spring force, the point S is the centre of gravity, and a is the gap between the cage and the sprag.

On the case of the lift-off X, the centrifugal force causes the sprag to lift-off from the outer ring. Therefore, the freewheel works wear-free, which leads to an unlimited life service. An example of the working system of the lift-off X can be seen in Figure 2.9.

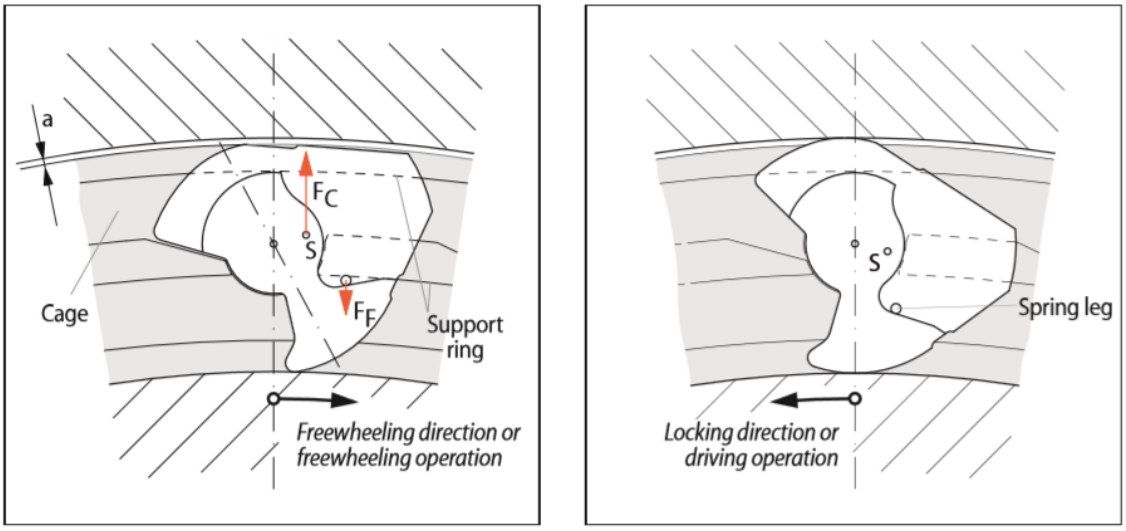

a b

Figure 2.9: (a) Sprag lift-off X in freewheeling operation, (b) Sprag lift-off X ready to be locked [8].

On the other hand, the lift-off Z's centrifugal force causes the sprag to lift-off from the outer race. The consequence is the same of the lift-off X, the freewheel works wear-free and it has a virtually unlimited life service. In Figure 2.10, a detail of the working system of the sprag lift-off Z can be seen.

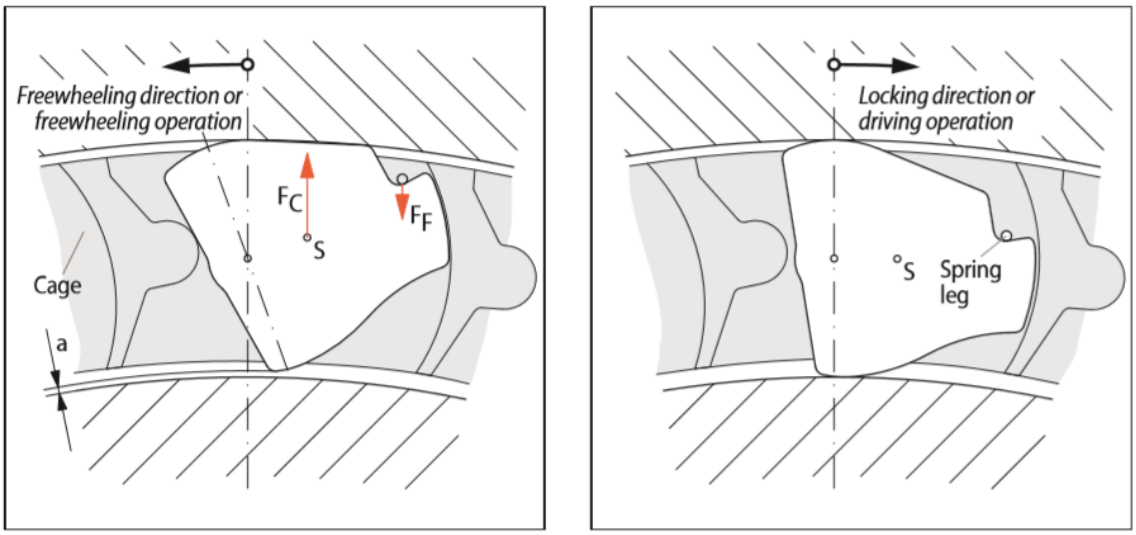

a b

Figure 2.10: (a) Sprag lift-off Z in freewheeling operation, (b) Sprag lift-off Z ready to be locked [8].

The type with hydrodynamic sprag lift-off is suited for overrunning at high speed for both, overrunning and driving operations. The driving speed can be as high as the freewheeling speed. In this case, the lift-off is produced by an oil flow, and the relative speed between the outer and the inner rings is crucial for the lifting-off function. These particular type of

freewheels include an oil pump based on the Pitot tube principle. In the Figure 2.11, the freewheeling operation and a detail of the Pitot tube and its pumping direction can be seen.

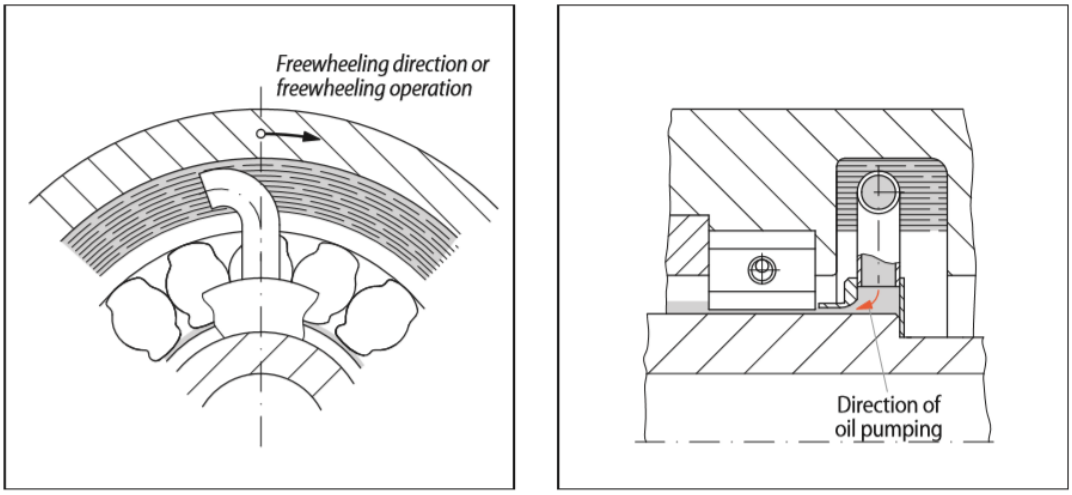

a b

Figure 2.11: (a) Hydrodynamic sprag lift-off in freewheeling operation, (b) Detail of the direction of oil pumping [8].

Depending on the relative speed between the inner and outer ring, the oil flows at an angle, and not axially, which creates a reaction force on the sprags that overcomes the contact force of the sprag springs, and the sprags lift off from the inner ring. If the relative speed between the inner and outer rings reduces, also the lifting force is reduced. Just before getting to synchronous running, the sprags are brought to rest on the inner ring and ready to lock, which guarantees immediate torque transfer once the synchronous speed has been achieved. These kind of clutches enables a virtually wear-free freewheeling operation, meaning that their useful life is increased considerably.

2.3.3 Cross Morse

This supplier offers two different kinds of sprag clutches: the conventional sprag clutches and the free overrun clutches. The main difference between the free overrun clutches and the conventional ones is found in the gravity centre of the sprags, which is offset to the pivot point. Because of this, while in the overrun mode the sprags are thrown out of contact with the stationary race, because of the centrifugal force, which leads to a decrease of the wear-off of the sprags. These clutches are suited for applications with long periods of freewheeling at high speed.

2.3.4 Stieber

Stieber has developed roller and sprag freewheels. For the sprag freewheels apart from the conventional sprag clutches, two different models have been developed: the DC design and the RSCI design.

The DC design has the particularity of including a large number of sprags and two concentric cages that control the clutches. The DC design can be seen in Figure 2.12. The double cage design allows synchronising the sprags, and they are also individually energized by a special spring. The torque transmitted is quite high compared to the space that it is required. The numbers that appear in Figure 2.12 are 1-Outer race, 2-Cage, 3-Spring, 4-Sprag, 5-Inner race.

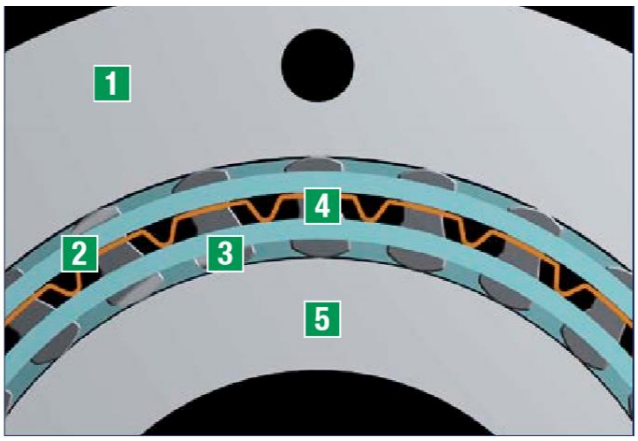

Figure 2.12: Detail of the DC design by Stieber [5].

The RSCI design is similar to the Cross Morse design, the centre of gravity of this sprag configuration offset to its rotation axis. Then, as the Cross Morse clutch, from the centrifugal force a lift off moment against an engaging spring is created. The sprag will tilt over to a contact free position when the centrifugal force is greater than the spring force. In Figure 2.13, the overrunning operation and the torque transmission can be seen.

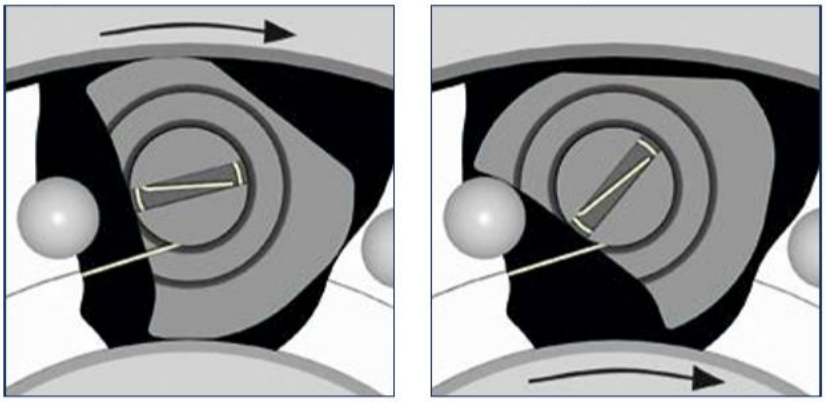

Figure 2.13: Detail of the RSCI design by Stieber. (a) Torque transmission (b) Overrunning operation [5].

2.3.5 Tsubaki

Tsubaki has been developing many different clutches during years, and those different clutches have culminated on their CAM clutch. This clutches have different parts: the inner and outer races, the bearing, the cam and the spring. In Figure 2.14, a scheme of the CAM clutch can be seen.

The inner and outer races have to have concentricity, and they hold the cams between them. This concentricity is maintained by the bearings that are used, and also the bearings have to bear he radial load. The most important element of these clutches is the cam, which is set regularly between the inner and outer race. This will lead to engagement or disengagement depending of the relative velocity of the inner and outer races. The final element that is used in Cam clutches is the spring, which assures that the inner and outer races are in contact at all times. The spring also assures that the load is spread across all cams when it is engaged.

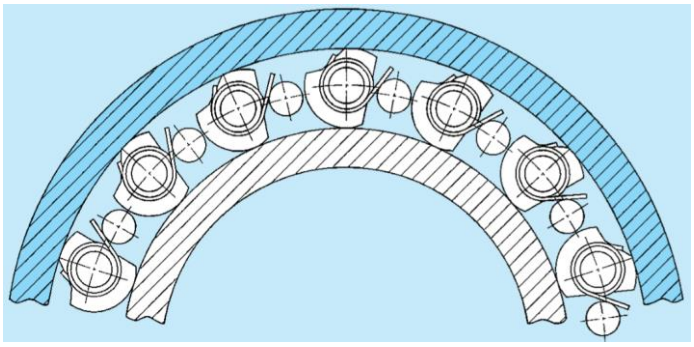

Figure 2.14: Tsubaki CAM clutch [13].

For overrunning applications, the cam locks the inner and outer races together when the cam clutch is stationary. However, when the inner race overruns at high speed, the cam is disengaged form the inner race. When the inner race begins to rotate slowly, the cam becomes again engaged. Finally, when the outer race is driven at low speed of rotation, the

cams drive the inner race at the same speed of rotation. In Figure 2.15, this process can be seen.

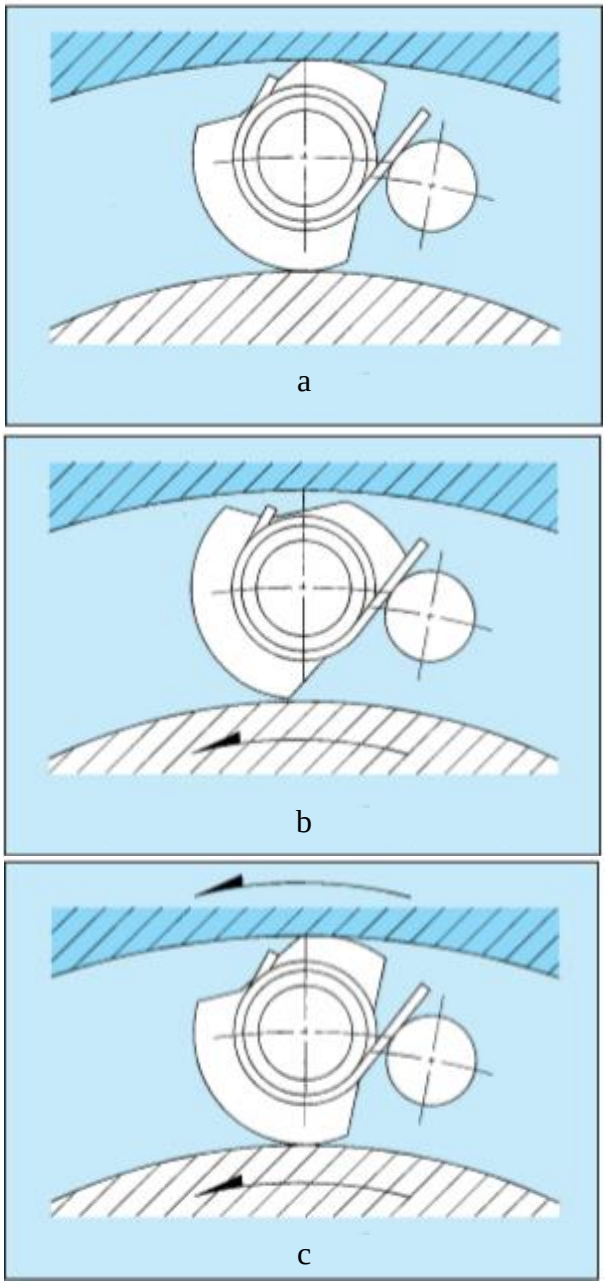

Figure 2.15: (a) Entire CAM Clutch is stationary (b) Inner race only turning (c) Inner and outer race locked and turning [13].

2.3.6 Renold

Renold offers two different types of sprags: the standard sprags and the ARO sprags.
The ARO sprags have a different shape than the standard sprags, as it can be seen in Figure 2.16.

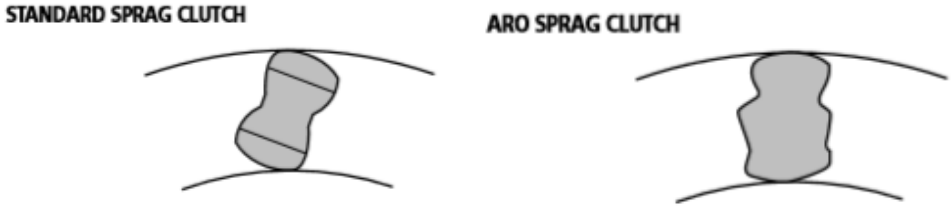

Figure 2.16: Detail of the shapes of standard and ARO sprag clutch shape [14].

These sprags are designed to resist the effects of overloads, high transient torque and vibration. In Figure 2.17 two conditions of ARO sprags can be seen: normal engagement and extreme overload conditions. In the normal engagement condition, the sprags work as a conventional sprag clutch. However, in the extreme overload condition the shape that is projected at the side of every sprag creates a positive sprag-to-sprag support, which allows the clutch bearing a higher torque, and it also helps both rollover and pop out.

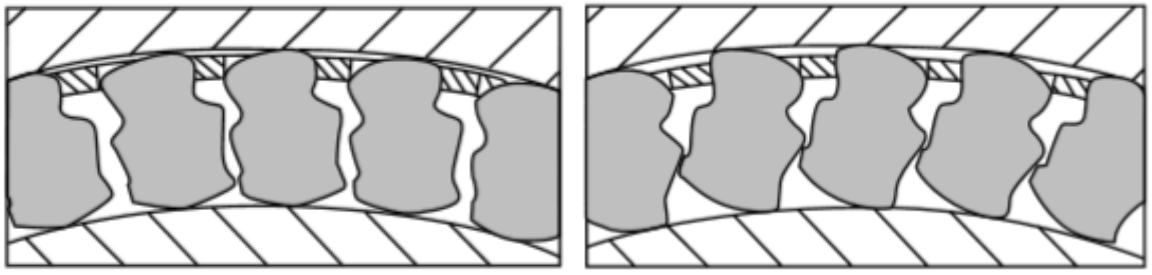

a b

Figure 2.17: ARO clutches conditions: (a) Normal conditions (b) extreme overload [14].

2.4 Description of the clutches used in the e-bike drive

As it has been remarked in chapter 1.1, three different clutches were used in order to design the e-bike drive. These three clutches were a GMN sprag clutch, a SUMA sprag clutch and a ratchet and pawl clutch.

There will not be any further comments about the SUMA sprag clutch, because its behaviour was supposed to be similar to the GMN clutch, however, the SUMA clutch brought many more problems with its assembly and the loads that it could bear were minor than the GMN's.

2.4.1 GMN sprag clutch

The GMN sprag clutch used was the model FE 453 M, as it has been stated in chapter 1.1, and has the characteristics of the Table 2.1.

Table 2.1 Characteristics of FE 453 M.

Variable	**Value**	**Unit**
d	45	mm
D	53	mm
W	12	mm
$\mathbf{T_{nom}}$	321	Nm
$\mathbf{n_{max}}$	3400	min^{-1}
m	0,0275	kg

Several differences about the shape of the actual sprag and the 3-D model given by the supplier GMN can be observed in Figure 2.18. These differences must be done in purpose by the supplier in order to the others competitors do not copy the same shape.

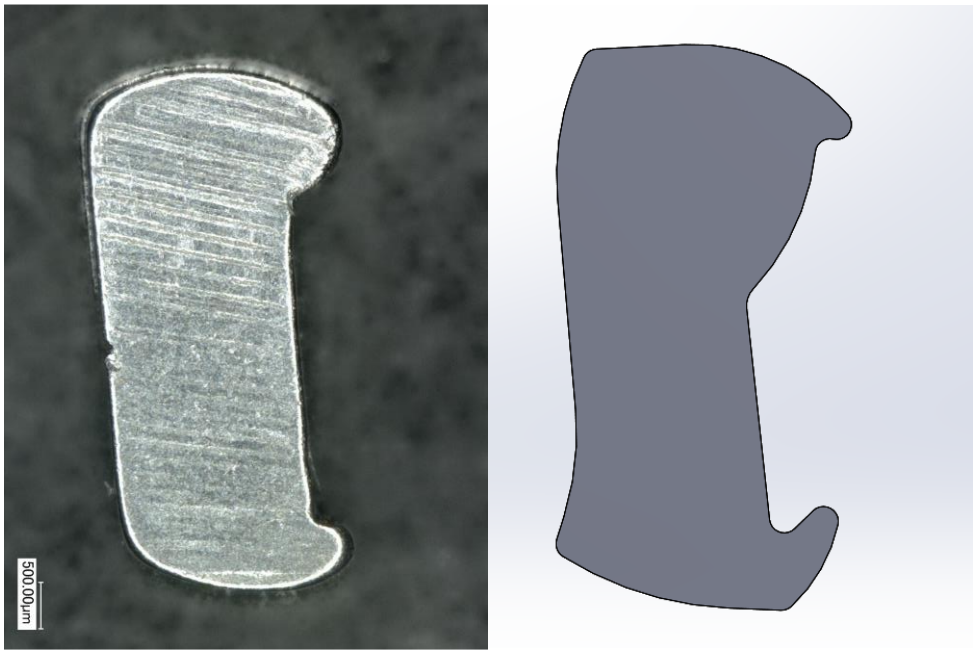

Figure 2.18: Comparison between actual and 3-D model sprag.

2.4.2 Ratchet and pawl clutch

This kind of clutch transfers the torque with its shape and not by friction, like the sprag clutch. Both the inner and outer parts were developed in LECAD. For confidentiality reasons, the final design will not be showed and a new one will be used.

This new design has the same working principle; therefore, the results that will be obtained will be useful to check for plastic deformation.

This clutch has three different parts: the inner hub, the pawl and the torque transfer ring. The three parts have the same material, structural steel and it has the properties that can be seen in Table 2.2.

Table 2.2: Ratchet and pawl material properties

Variable	**Value**	**Unit**
Material	Structural steel	/
Model	Linear elasticity	/
Density	7850	kg/m^3
Young's Modulus	200000	MPa
Poisson coefficient	0,3	/

The torque transfer ring has 30 ratchet teeth, and for the pawl, two different models will be used, the first one with three pawls and the second one with six pawls. Both pawls options will be distributed regularly. In Figure 2.19, the three-pawl design can be seen.

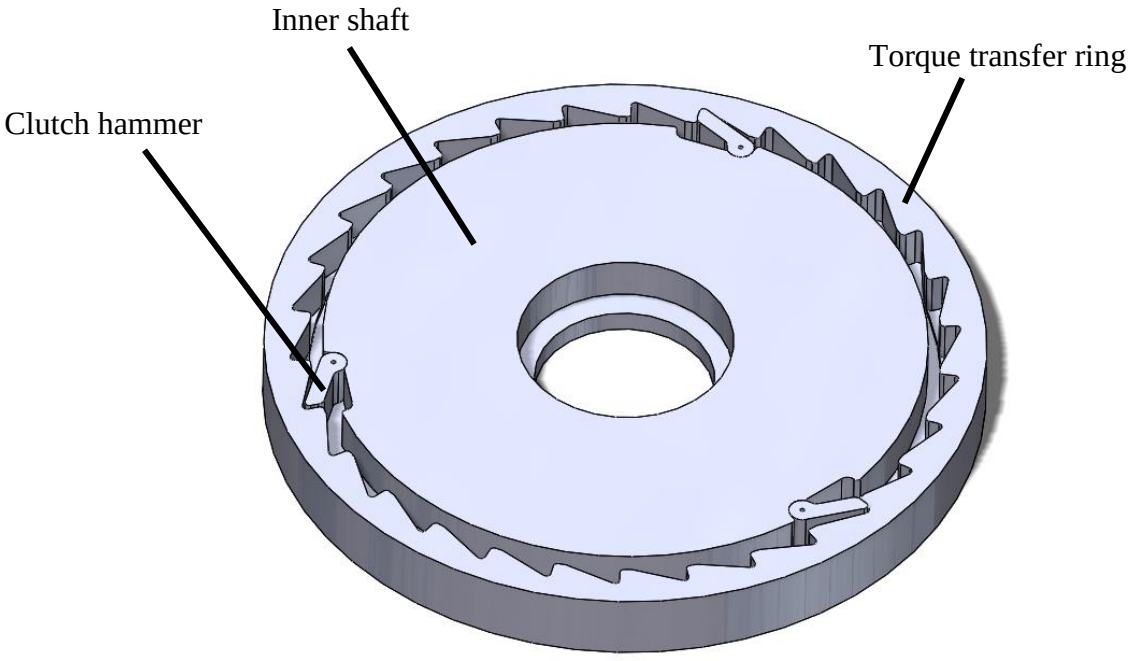

Figure 2.19: Components of the ratchet and pawl clutch.

3 Methodology

In order to compare the two different clutches some simulations with the ANSYS software, using FEM, will be done. For each clutch different simulations will be done. These simulations will have different loads, having cases with ideal conditions and other cases with more pessimistic or real conditions. First, the simulation of the GMN sprag clutch will be done, and after these, the ratchet and pawl clutch simulations will be seen.

The main purpose of doing the simulations on the sprag clutch is to observe the deformation that appears on the cage surface that is in contact with the sprags. Also, the stress values of the clutch will be checked. Later, the acceptable deformation will be discussed.

On the case of the ratchet and pawl clutch, the main reason to make the simulations is to obtain values for the stress. Then, the stress should be compared to the plastic deformation of the material, and check if the design can work without the appearance of plastic deformation. Nevertheless, the deformation will also be checked, in order to verify if the clutch has an evenly distributed load.

Once the simulations are done, comparison between the two types of clutches should be done. This comparison will be done comparing the mass used in each case, in order to know from the designs that can bear the loads, which is the lighter, therefore, more appropriate for being used as an e-bicycle clutch.

3.1 Sprag clutch simulations

Before doing the simulations, the calculations about the torque and the tangential forces that appear on the clutch must be done. For doing the calculations a scheme of the torque and the forces that the outer cage receives from the sprags can be seen in Figure 3.1. Each sprag generates a normal force and a tangential force to the outer cage of the clutch. With the tangential force, the torque is created.

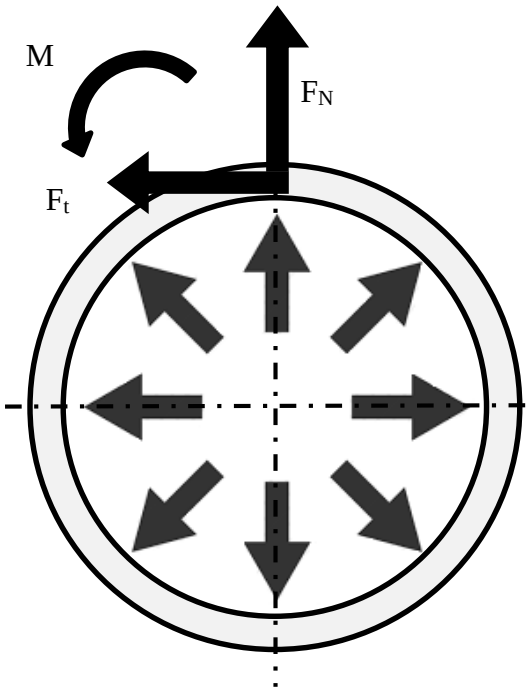

Figure 3.1: Forces and torque scheme.

As it has been said, F_t is the tangential force, F_N is the normal force, M is the torque, D is the outer diameter, μ is the friction coefficient, p is the pressure that the sprag is pushing and A is the area of the sprag. In order to calculate the pressure and the forces that appear on the clutch, the torque is considered 300 Nm. With this information and the next equations, the forces, F_t and F_N can be calculated.

$$M \leq F_t \cdot \frac{D}{2} \tag{3.1}$$

$$F_t = F_N \cdot \mu \tag{3.2}$$

$$F_N = p \cdot A \tag{3.3}$$

Once the equations are set, knowing the outer diameter, D, that is 53 mm, and assuming a friction coefficient for the worst case scenario, μ, for the worst case scenario as 0,12 [15], because the contact is between two steel surfaces that are lubricated, the F_N can be calculated and a value of 94,34 kN is gotten.

Then, in order to calculate the pressure, p, the contact area has to be determined. The suppliers assert that only between 50% and 75% of the teeth on the sprag clutch are working

when they are transmitting the torque. Two cases will be simulated: worst-case scenario and best-case scenario.

The worst-case scenario is the one where approximately 50% of the sprags will be working. This assumption leads to a use of 26 out of 51 sprags that the clutch has. In addition, for the position of the sprags working, the greater values of displacement will be given by symmetrical forces like the ones that appear on Figure 3.2, the surfaces marked with green colour represent the sprags working where the pressure is applied.

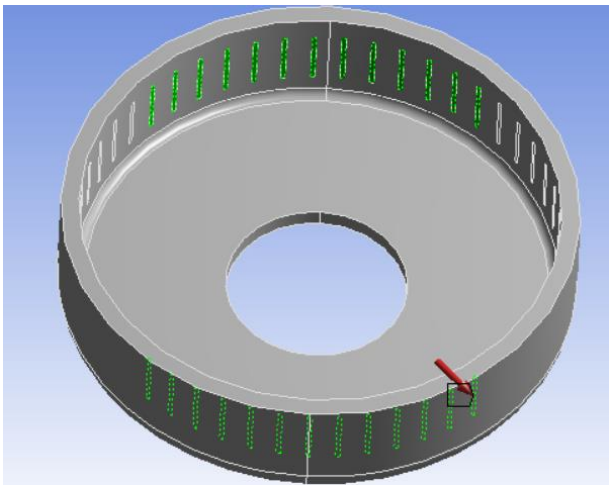

Figure 3.2: Application of the F_N in the worst-case scenario.

The best-case scenario that will be simulated is when all the sprags are working, it is known that this is not a real situation, but it will give a comparison point on how much deformation difference will there be.

To get the values of the pressure that affects the clutch, the contact area of the sprags has to be set. Some reasonable assumptions have been made, such as that from the 9 mm of the length of the sprag only 7 mm are in contact with the outer cage. And for the width, about 0,8 mm of the sprag are in contact with the outer cage surface.

With these values of height and width and considering the area as a rectangle, the pressure can be calculated. Leading to values of 330,32 MPa for the best-case scenario and 647,93 MPa for the worst-case scenario.

Once the pressure values have been calculated, it is turn for the accepted deformation to be determined. This acceptable deformation will be determined using a geometric method. This method could be used thanks to the geometric description done by Huang Chang et al. [16].

Using the image of the sprag clutch and the software AutoCAD to extend the geometric lines, the difference between the freewheeling position and the transferring torque position is possible to see. In Figure 3.3, the blue lines represent the sprag when it is transferring torque, the black lines represent the sprag while it is in the freewheeling position, and the red line represents the eccentricity that leads to the torque transference.

The difference between the two dimensions, freewheeling and torque transfer, is 0,182 mm. For this difference of distance between the two possible positions for the clutch, freewheel and torque transfer, it is supposed that the accepted tolerance for the clutch deformation is around 0,1 mm.

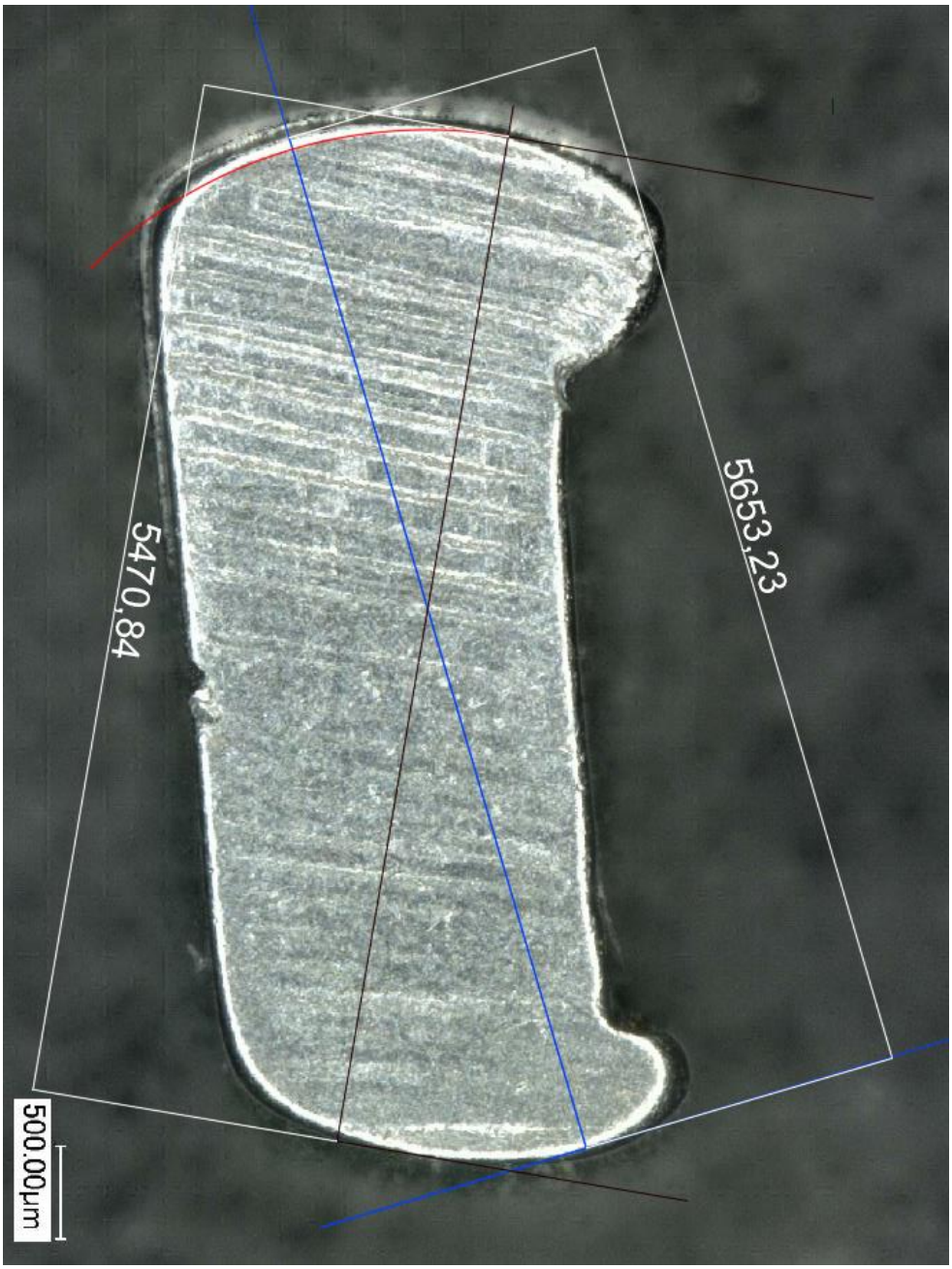

Figure 3.3: Geometric analysis of the sprag.

After looking with detail the sprag, it can be said that the geometry that is more important on its design are the upper and lower part of the sprag, both surfaces are in contact with the clutch. The design of both of the parts are important because they establish de contact

distance and the contact zone with the clutch. Moreover, the eccentricity that is designed on the upper part, allows the clutch to either work on freewheeling or torque transferring.

The design of this sprag, allows obtaining a great normal force for a little tangential force. The proportion of these two forces is showed in Figure 3.4. As it can be seen, the geometry of the sprag help the torque transmission. It is like the mechanism of a wedge. It uses a mechanical advantage by relating its length with its width. The relationship between the tangential and the normal force is given by the angle α_0.

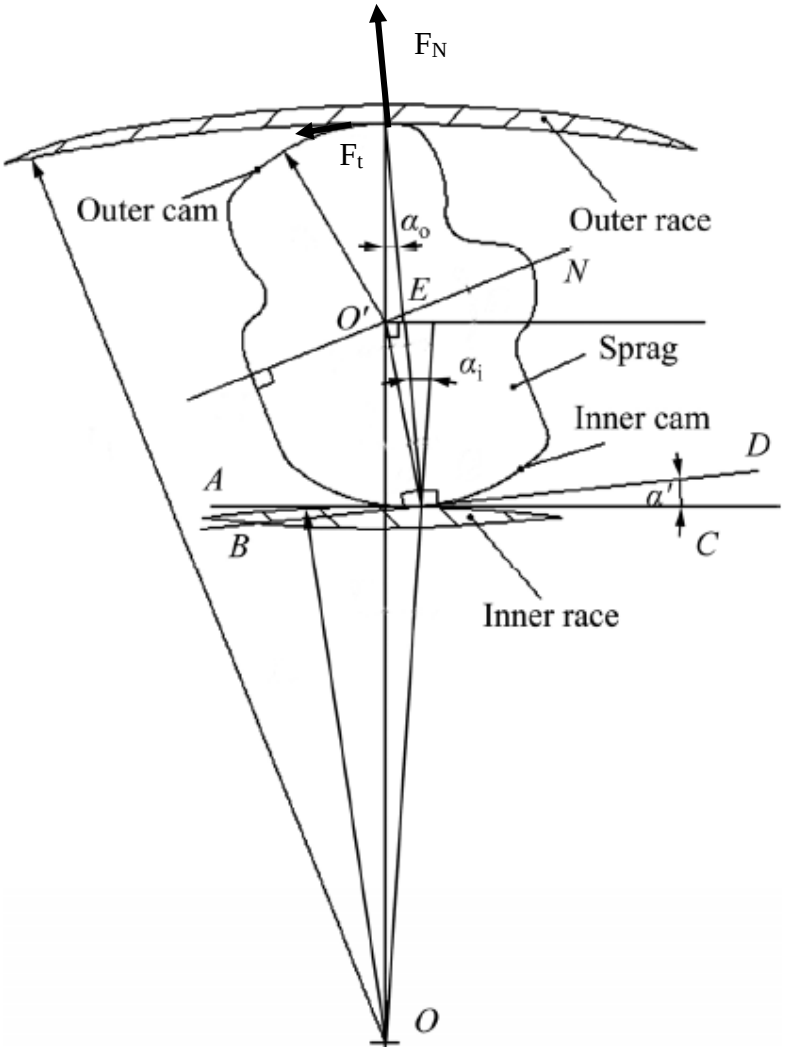

Figure 3.4: Sketch of the relation between tangential and normal force. [17]

The design of the sprag could be modified in order to increase the deformation accepted in this clutch. The problem of modifying this sprag is that it needs some conditions to work properly. The main condition for the torque transfer is the one shown in equation 3.4.

$$M = F_t \cdot \frac{D}{2} \tag{3.4}$$

$$F_t < F_N \cdot \mu \tag{3.5}$$

The best option considered to increase the deformation accepted is to increase the width on the upper part of the sprag, this way the eccentricity will keep on going and the sprag will have to rotate more to be able to lock the clutch. It is important that the design has the same force relation between the tangential and the normal force. If this relation is not kept, the force needed will be higher, therefore, the clutch will not work properly. This option may lead to redesign the clutch by reducing the number of sprags, because each of them will need more space.

Once proper values of deformation are gotten, the stress values will be checked in some selected designs. In this way, it will be seen if both criteria of deformation and stress are met. The criteria for the stress is that this should be below the elastic limit of the material.

3.1.1 Simple cage simulation

In order to do the simulations, as it has been said before, they will be done from the simplest cases to the more complex ones. That is why, for the first set of simulations, only the outer case will be studied, and the thickness between the inner and outer diameter will be increased in order to verify how the stiffness affects the cage deformation.

The geometry of the clutch has been created with the software SolidWorks and an example of the geometry can be seen in Figure 3.5. The corners of the clutch have been rounded to avoid high stress in that part. The parameter t is the one that has been changed in order to modify the thickness and the stiffness of the clutch.

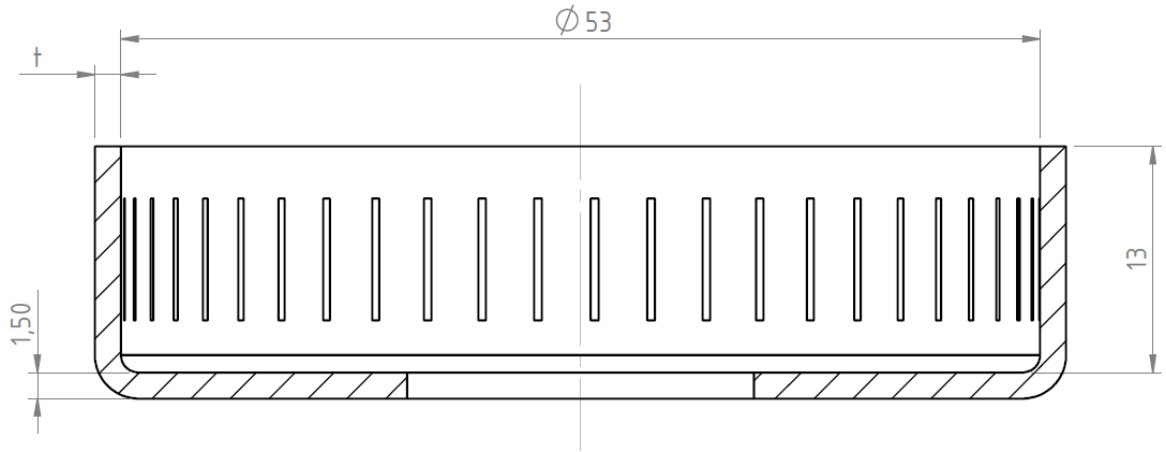

Figure 3.5: Sketch of the clutch used in the first set of simulations.

To do this set of simulations only one support was required. A fixed support was set on the inner ring. It is meant to recreate the impossibility of the cage to be deformed because of the

axis that will transmit the torque to the wheel. An example of the boundary conditions and the loads applied in the worst-case scenario can be seen in Figure 3.6

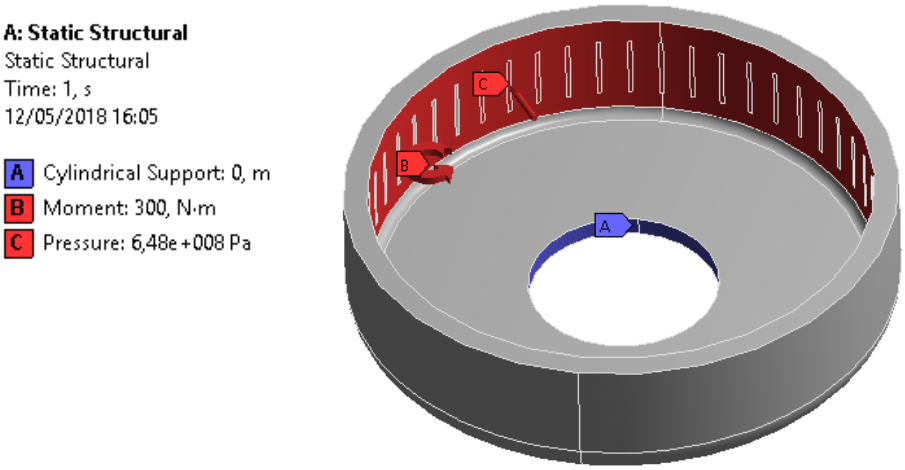

Figure 3.6: Boundary conditions and loads applied in the worst-case scenario.

3.1.2 Double-cage simulation

For the next set of simulations, an outer cage will be added to the previous simulation. Therefore, there will be another part making the whole clutch stiffer. The purpose of adding an outer cage is that a greater stiffness of the cage will be achieved while trying to have a cage as lighter as possible.

In this set of simulations, an assembly of the inner and the outer cage will be used. The software ANSYS has different options to create the boundary conditions. In this case two of them will be used, the frictional and the bonded.

The bonded connection is the one that ANSYS software sets by default. It would simulate the assembly like both of the cages, the inner and the outer, were welded together. On the other hand, the frictional connection is more realistic, because it lets the two cages rotate if the sliding force is greater than the frictional force.

The frictional connection takes more time to simulate, so, both cases will be simulated. When the simulations are done, both cases will be compared and if the results are similar, only the bonded connection will be simulated in future simulations. Therefore, time will be saved in further simulations, however, if the results are not similar, frictional connection simulations will be done from then on.

Different geometry cases have been created to check which the best ones are. Three different inner cages have been designed. In each case, the thickness of the wall is different. The designs have thickness of 1 mm, 1,5 mm and 2 mm. A sketch of the inner cage can be seen in Figure 3.7, where the D value is changed to 55, 56 or 57 to modify the wall thickness.

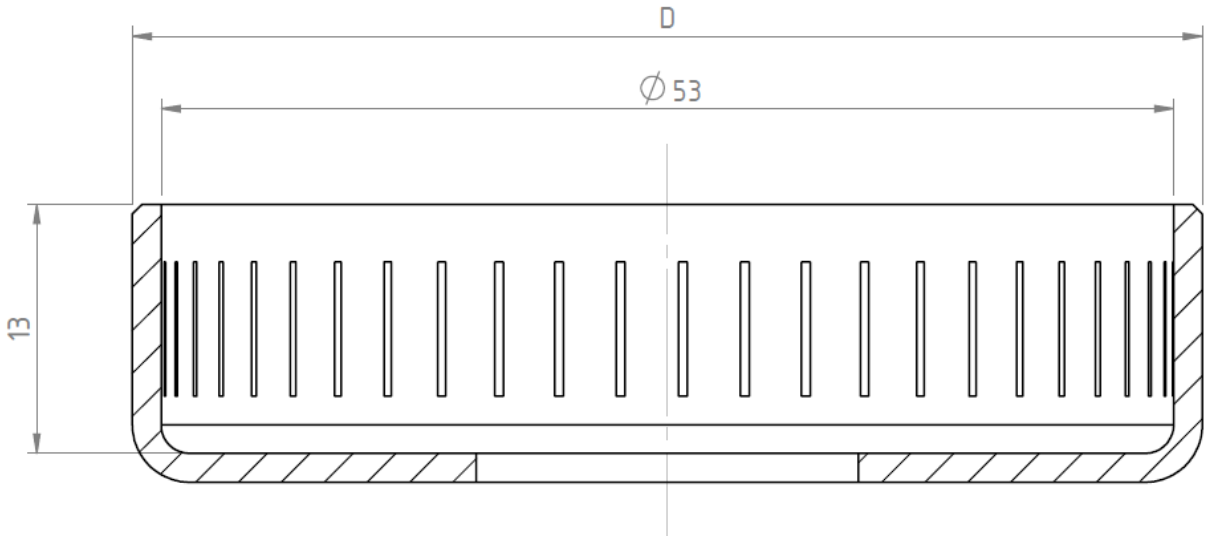

Figure 3.7: Sketch of the inner cage.

Also for the outer cage, different geometries have been created. In this case, the different dimensions are the length of the wall and the inner diameter to fit each inner cage correctly. The length of the wall for the different outer cages are 10 mm, 7 mm and 4 mm. A sketch of the outer cage can be seen in Figure 3.8. In this case, three different parameters are used: L for the length of the wall, D_{int} for the inner diameter, which will match the outer diameter of the inner cage, and D_{ext} for the outer diameter, which will be 3 mm greater than the Dint in order to have a 1,5 mm wall.

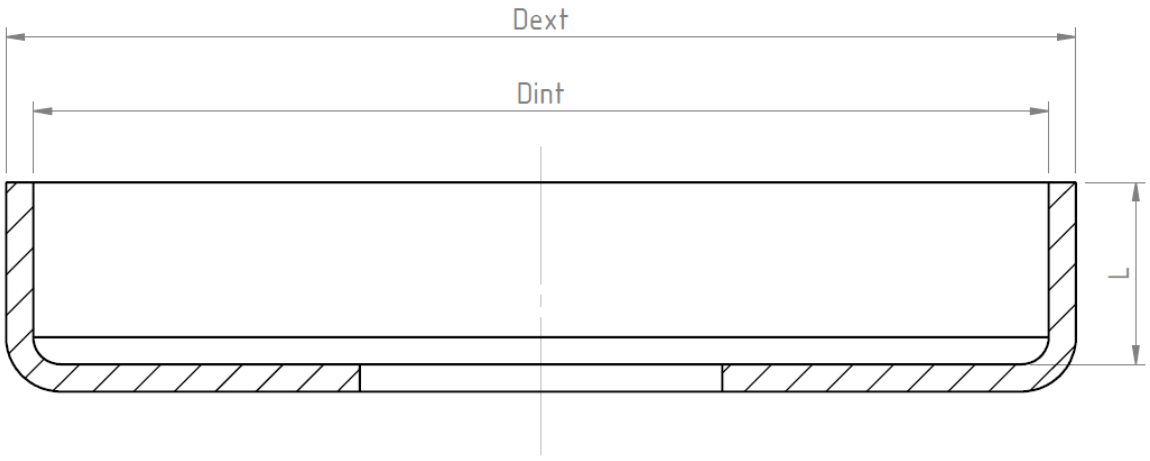

Figure 3.8: Sketch of the outer cage.

To summarize this chapter, 18 different cases will be studied. First nine cases with the characteristics shown in Table 3.1 with the bonded connection, and after those simulations, the same geometry will be used for the frictional contact.

Table 3.1: Geometry characteristics of the study cases.

	Thickness [mm]	Length [mm]	Weight [g]	Nodes
Case 1	1	10	78,43	46083
Case 2	1,5	10	97,04	51176
Case 3	2	10	107,58	54234
Case 4	1	7	72,16	44408
Case 5	1,5	7	90,66	49494
Case 6	2	7	101,09	52578
Case 7	1	4	65,89	42307
Case 8	1,5	4	84,27	46925
Case 9	2	4	94,60	50232

The boundary conditions set in these simulations are two cylindrical supports where the shaft should be, one for the inner part an another one for the outer part of the clutch. They are set to prevent the movement of the cage and recreate the constraints that appear in real life. The loads applied are a torque of 300 Nm and a pressure applied to the required sprags of 648 MPa, as in the simple cage simulation. An example of the boundary conditions and loads applied at this set of simulations can be seen in Figure 3.9.

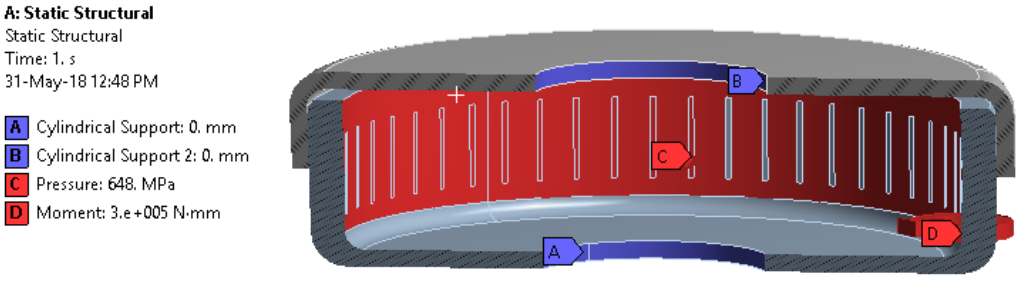

Figure 3.9: Boundary conditions and loads applied to double-cage simulations.

Those first nine cases will be simulated first, however, if there is need in doing more simulations, because the maximum deformation gotten is higher than the accepted, more designs will be made in order to perform these new simulations. It will be decided then which designs options can be avoided, in order to save time and resources.

3.1.3 Alternative solutions

In this subchapter, different solutions will be explained. These solutions are explained apart because they are more complicated to fabricate, so probably, it may not be justified to pay a higher price for the little improvement that can be achieved on the cage's stiffness.

The first case considered was adding some ribs to the outer-cage in order to difficult the bending of the cage itself. However, this design is complicated to make. Therefore, an alternative has been proposed. This alternative consists on having a tighter wall on the outside part of the clutch. This works as a reinforcement and should difficult the bending of the cage wall. A sketch of this alternative can be seen in Figure 3.10.

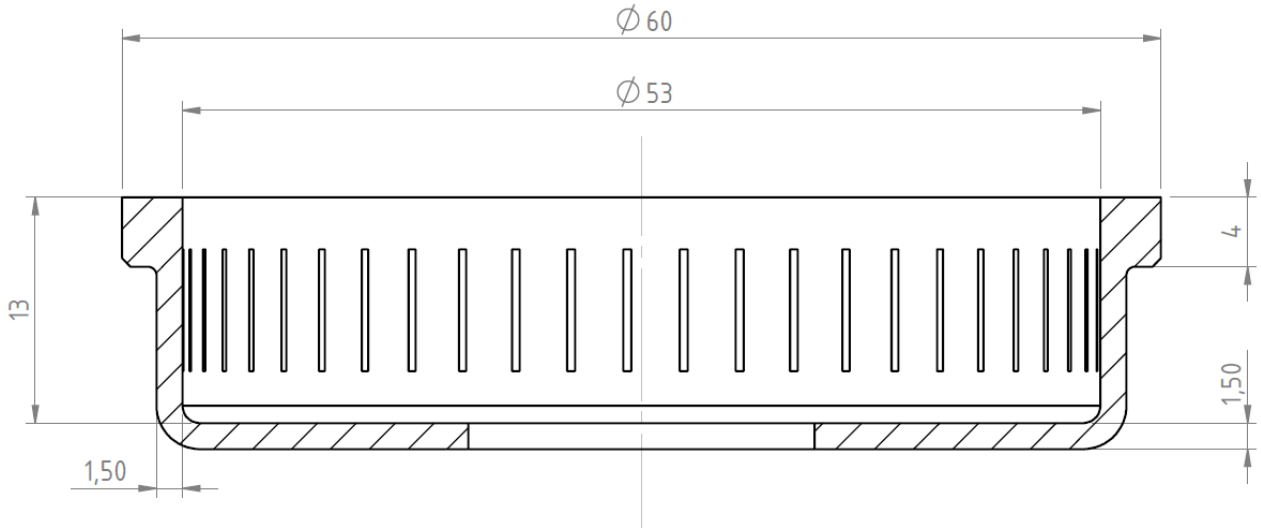

Figure 3.10: Sketch of the design with a tighter wall.

One other possibility to increase the stiffness is to design the outer wall in order that it has an inclination. This inclination should be thicker on the outer part of the cage. This way the clutch could be made by founding or by turning. In Figure 3.11 a sketch of the design can be seen.

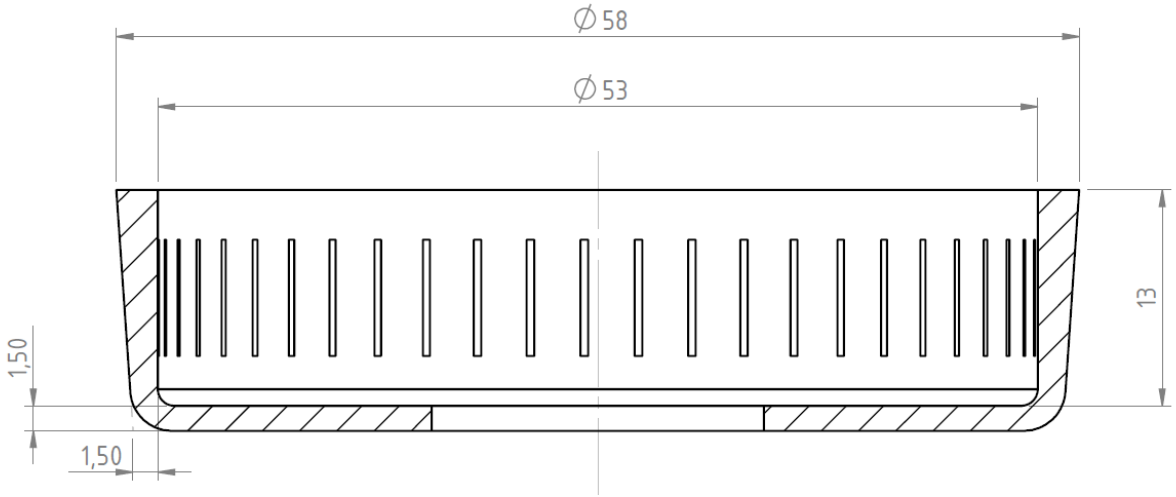

Figure 3.11: Sketch of the design with the inclined wall.

3.2 Ratchet and pawl simulations

In this case, the deformation that the clutch receives when applying a certain load is not as important, because the torque is not transferred by friction, but by shape. Therefore, the focus of the simulations is that the clutch does not suffer plastic deformation, not even in the interior or the exterior part of the clutch.

If there were any plastic deformation, it would mean that the shape of the outer clutch or the pawl of the inner part of the clutch have changed their shape permanently, which would mean that the torque will not be transferred correctly. The plastic deformation can also lead to the breakup of one of those parts.

Usually, the inner part is designed with three pawls; however, other designs have six of them. The number of pawls that are used in the clutch is important because it will affect the force that the cage receives. On Figure 3.12, a sketch of the forces that appear on the clutch is shown.

On the equations that follows, M is the torque that has to be transferred, F is the force that will transfer the torque, s is the distance from the centre of the clutch to the application point on the outer cage, n_p is the number of pawls, and F_p is the force that each pawl will do to transfer the torque. The torque is 300 Nm like in the sprag clutch simulation. The distance between the midpoint of the surface where the force is applied and the centre of the clutch, s, is 36,25 mm. Therefore, the force applied can be calculated with the next equations:

$$M = F \cdot s \tag{3.6}$$

$$F_p = \frac{F}{n_p} \tag{3.7}$$

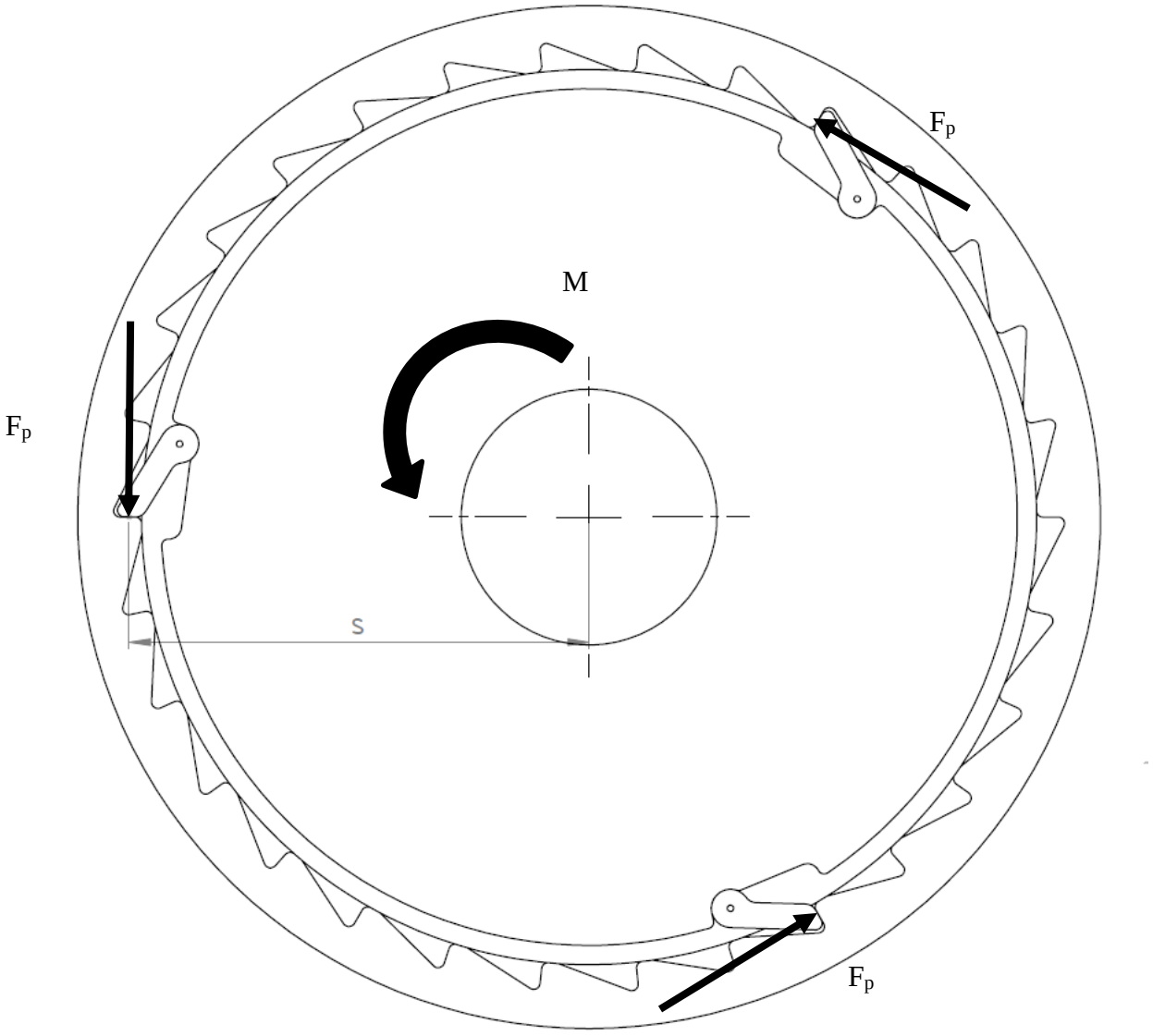

Figure 3.12: Sketch of the ratchet and pawl clutch loads.

Once used the equations a force of 2759 N is obtained for the case of the three pawls and 1379 N for the six pawls case.

The force that will receive the inner cage will be the same as the outer cage; however, it will be set on the opposite direction.

Once the force has been obtained, two different simulations will be done. First, the outer cage simulations, and later the inner cage simulations. On both cases, the purpose of the simulations, as it has been said before is to check if with the design there is plastic deformation, which could lead to malfunction or even to a breakout of the clutch.

After the simulations are completed, the difference between the tolerances of the design and the deformation have to be checked. Because if the tolerances of design are greater than the

deformation gotten, the hammers will not work all at the same time, therefore, the stresses obtained will be higher and the material could get to plastic deformation much easily.

3.2.1 Outer part simulation

As it has been said before, two different simulations will be done for the outer cage. The first simulation will be the one with the design with three pawls, and the second simulation will be the one with the design with six pawls.

The design of the outer cage will be the same for both simulations; the only change on the simulation will be the number of applied loads. The boundary conditions set in these simulations, as well as in the other simulations, is a cylindrical support on the inner part of the clutch. The loads are applied every 120º for the three-pawl simulation and every 60º for the six-pawl simulation. A scheme of the application of the loads and the boundary conditions for the three-pawl simulation can be seen in Figure 3.13.

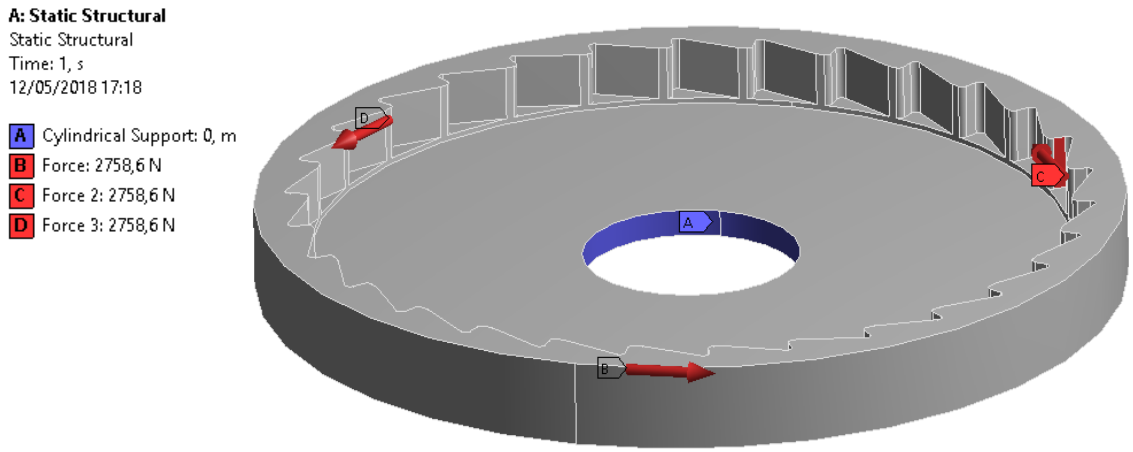

Figure 3.13: Boundary conditions and loads applied on the three-pawl simulation.

3.2.2 Inner part simulation

For the inner cage simulation, a design of the inner part of the cutch has been created. The design created is the following that can be seen in Figure 3.14. As it can be seen, this assembly is formed by four different elements: three pawls and the inner part.

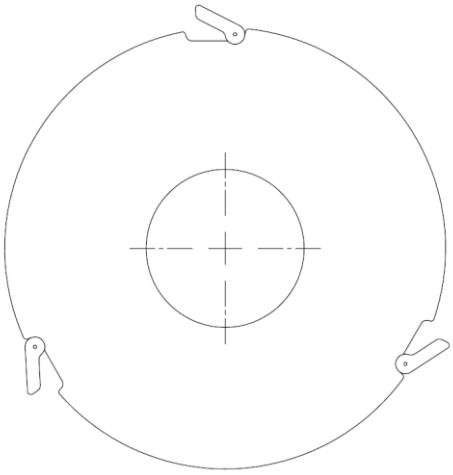

Figure 3.14: Sketch of the inner part of the cage.

Not all the inner cage will be studied. The study will be focused on the most characteristic element, which is the pawl or hammer that will transmit the torque. The forces that it will receive will be the same that in the outer cage, however the force will be on the opposite direction. Therefore, the force that will receive each hammer will be 2759 N in the case of the three pawls and 1379 N in the case of six pawls, as it has been calculated before.

The boundary conditions are the same as the previous case, a fixed support on the inner ring of the shaft. A sketch of the application of the loads and the boundary conditions can be seen in the Figure 3.15.

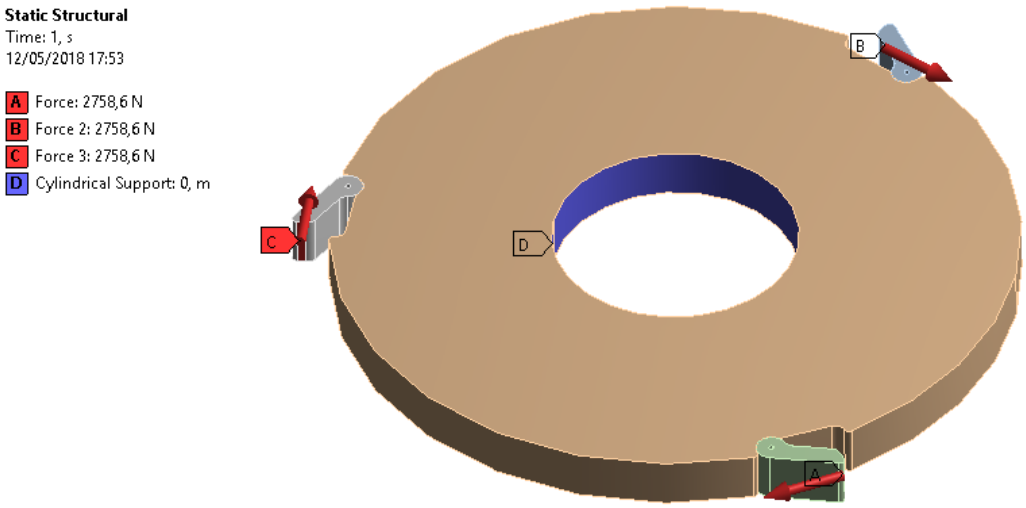

Figure 3.15: Boundary conditions and loads applied at the three-pawl simulation.

Apart from doing the simulation of the inner cage assembly, the simulation of only the pawl hammer will also be done. It will be done in order to check the results that will give the previous simulation, and to verify the contact setup.

The boundary conditions for the hammer simulations are a fixed support on the outer part of the hammer. It was also considered to fix only the pin hole, however, using this boundary conditions high stresses appeared on the pin hole. The load applied is the same as the previous case. A detail of the boundary conditions and the load applied can be seen in Figure 3.16. In Figure 3.17, the sketch of the hammer can be seen, and also, the relation between the surface where the load is applied and the other faces of the hammer is shown.

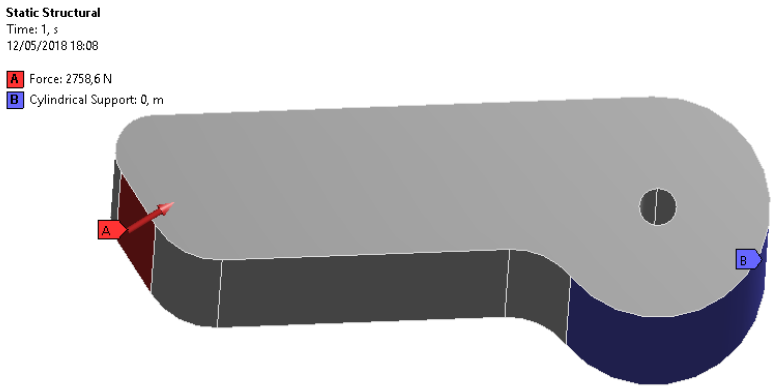

Figure 3.16: Boundary conditions and load applied for the hammer simulation.

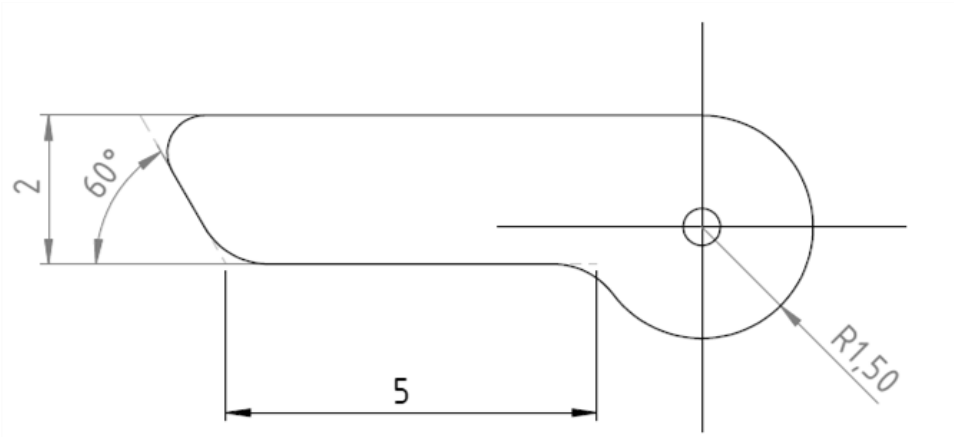

Figure 3.17: Sketch of the hammer.

4 Results and discussion

4.1 Sprag clutch results

4.1.1 Simple cage results

The simple-cage simulations have been done using a static structural simulation, and the material used is structural steel with a Young's modulus of 200 GPa and a Poisson's coefficient of 0,3. The model used is a linear elasticity model. The mesh was created by using a quadratic element order, and curvature function for the sizing.

Seven different geometry cases have been simulated in this chapter. Each case with its both scenarios explained before: the best-case with all the sprags working and a pressure of 330 MPa and the worst-case with only half of the sprags working and a pressure of 647,93 MPa. In addition, a 300 Nm torque is applied in both cases. The results of the deformation are found at the Table 4.1.

Table 4.1: Deformation values for the simple cage simulations.

			Best-Case	Worst-Case		
	Thickness [mm]	Number of nodes	Max. Deformation [mm]	Max. Deformation [mm]	Max. Y Deformation [mm]	Max. Z Deformation [mm]
Case 1	1	36 331	0,215	25,206	22,158	21,919
Case 2	1,5	48 439	0,150	6,724	5,786	5,796
Case 3	2	58 181	0,103	2,815	2,432	2,400
Case 4	2,5	63 088	0,084	1,842	1,498	1,548
Case 5	3	66 645	0,075	1,270	0,973	1,054
Case 6	3,5	69 635	0,068	0,919	0,715	0,752
Case 7	5	74 061	0,070	0,491	0,364	0,361

As it can be expected, the greater the thickness the lesser the deformation. The maximum deformation is given where the pressure is applied on the worst-case scenario, as it can be

seen in the Figure 4.1. On the other hand, on the best-case scenario the maximum deformation is given on top of the wall, as it can be seen in Figure 4.2. On those images, the deformation has been exaggerated to get a better view on which part the deformation occurs.

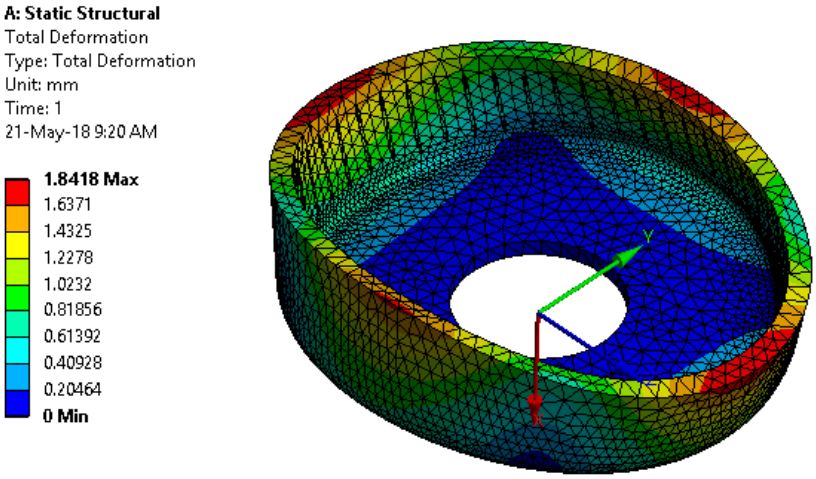

Figure 4.1: Maximum deformation on worst-case scenario for case 4.

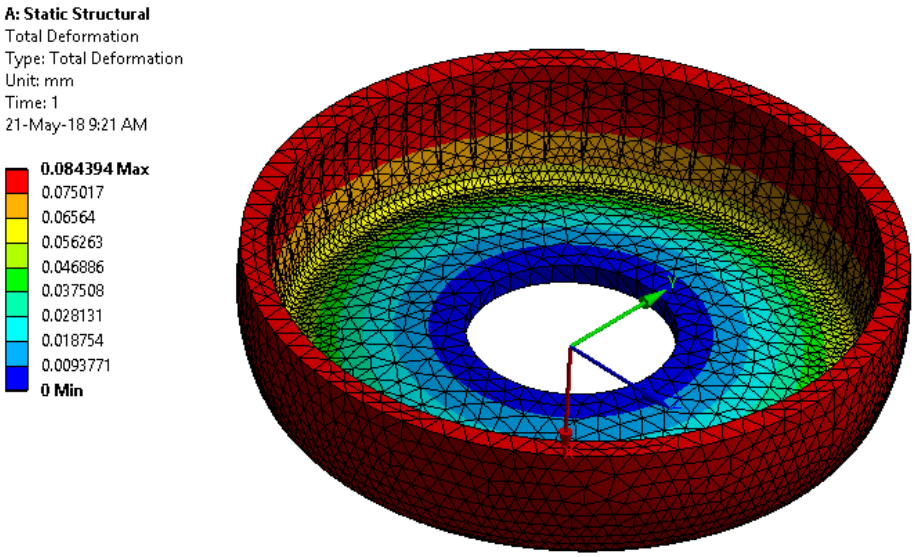

Figure 4.2: Maximum deformation on best-case scenario for case 4.

In Figure 4.3, a comparison between the results of the studies made is shown. Of course, the worst-case scenario gives greater values of the deformation, this is because the fact that the loads are not regularly distributed on the clutch, as if they are in the best-case scenario. Moreover, in this graph, for the worst-case scenario, a great decrease of the maximum deformation is given by just increasing the thickness of the wall, like a negative exponential function.

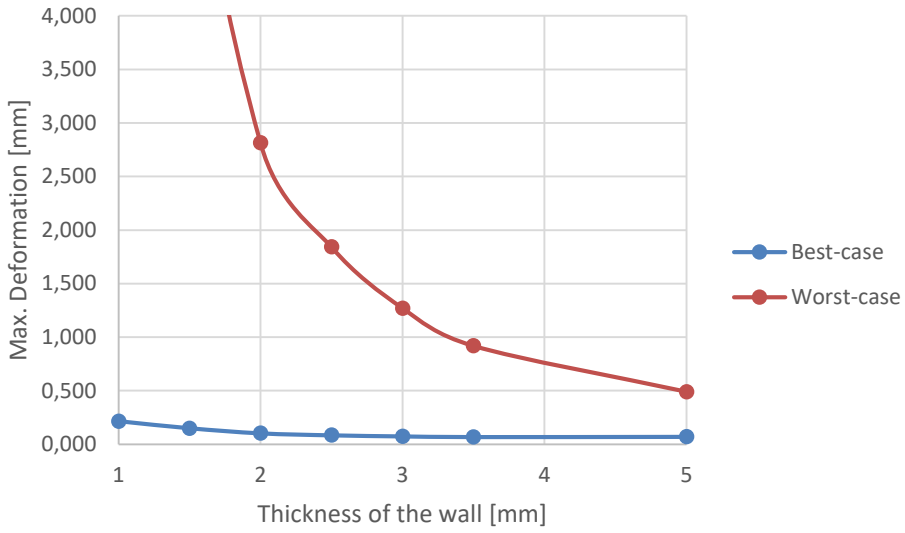

Figure 4.3: Comparison between the deformations of the cases studied.

The first thing it is possible to say with this first set of simulations is that there is an important difference between the two cases studied. To have the best approximation, only the worst-case scenario will be simulated form now on, this way time will be saved, and more simulations will be able to be done.

Moreover, a great deformation is gotten after applying the transmitting torque. This deformation can become a problem if it is too big, because one of the sprags could turn the other way and lock the mechanism. This would mean that the clutch would not run in freewheel mode anymore.

Obviously, the greater the thickness, the greater the stiffness of the clutch. The ideal clutch would be one that would not get any deformation because of the load. In order to reach this an infinite thickness of the clutch wall would be needed, however, it would mean an infinite weight, and of course, the bicycle would not work. Due to this, a balance between weight and stiffness shall be found.

4.1.2 Double-cage results

The double-cage simulations have been done like the simple-cage simulations: using a static structural simulation, and the material used is structural steel with a Young's modulus of 200 GPa and a Poisson's coefficient of 0,3. The model used is a linear elasticity model. The mesh has also been created by using a quadratic element order, and curvature function for the sizing. However, in these simulations, as it has been explained, there will be two different sets of simulations, one with bonded contact and one with frictional contact.

For the bonded contact, the different details of the contact region will be set as program controlled, because it is known that with these settings the simulation works fine. On the other hand, for the frictional contact the details of the contact region have been modified, because the software usually works better with different settings for this kind of simulation. Therefore, the advanced formulation has been set as an augmented Lagrange formulation, which is used for non-linear solid body contact of faces. The detection method has been set on Gauss point; the normal stiffness factor has been set on 0,1 because it is useful for bending-dominated situations. In addition, the interface treatment has been set to adjust to touch, this way the software will determine the needed amount of offset to close the gap between the two bodies and establish initial contact. To create this type of contact a frictional coefficient of 0,2 has been used. This value has been chosen because we are dealing with a steel-steel contact without lubrication [15].

As it has been stated in chapter 3.1.2, two sets of simulation were done, the first with bonded contact, and the second with frictional contact. For each set of simulations, the length and the thickness have been changed. The bonded contact results can be seen in Table 4.2.

Table 4.2: Deformation values of the double-cage simulations with bonded contact.

	Thickness of the wall [mm]	Length [mm]	Nodes	Max. Deformation [mm]	Max. Y deformation [mm]	Max. Z deformation [mm]
Case 1	1	10	46083	0,182	0,090	0,181
Case 2	1,5	10	51176	0,114	0,061	0,109
Case 3	2	10	54234	0,087	0,050	0,082
Case 4	1	7	44408	0,251	0,114	0,251
Case 5	1,5	7	49494	0,157	0,129	0,123
Case 6	2	7	52578	0,114	0,058	0,108
Case 7	1	4	42307	0,284	0,137	0,281
Case 8	1,5	4	46925	0,202	0,092	0,193
Case 9	2	4	50232	0,129	0,063	0,124

The comparison between the values of the bonded contact simulations can be seen in Figure 4.4. From this figure, we can conclude that both the thickness of the wall, and the length of the outer cage affects to the stiffness of the clutch. However, the thickness is more determinant for the stiffness.

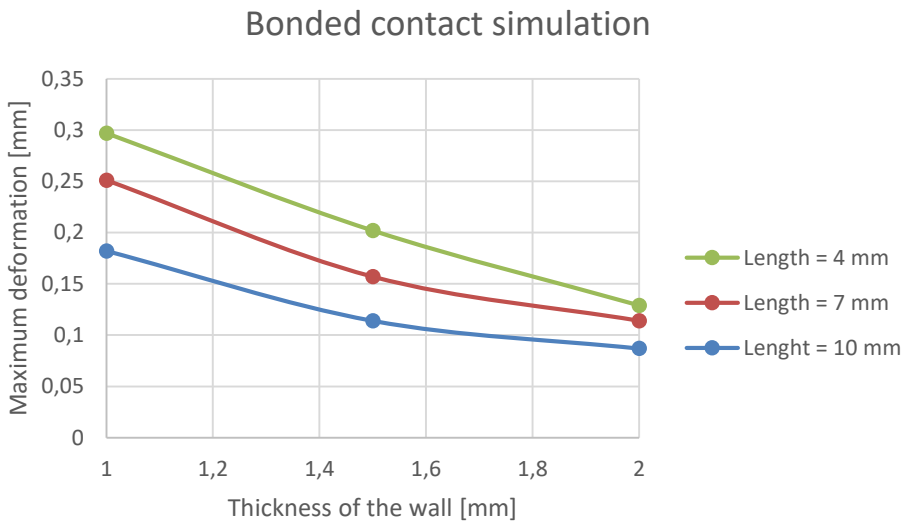

Figure 4.4: Bonded contact simulation results.

Once the bonded contact simulations have been done, the same simulations but with frictional contact have been done. The results obtained can be seen in Table 4.3.

Table 4.3: Deformation values of the double-cage simulations with frictional contact.

	Thickness of the wall [mm]	Length [mm]	Nodes	Max, Deformation [mm]	Max, Y deformation [mm]	Max, Z deformation [mm]
Case 10	1	10	46083	0,660	0,551	0,434
Case 11	1,5	10	51176	0,392	0,350	0,264
Case 12	2	10	72730	0,472	0,359	0,328
Case 13	1	7	86785	1,019	0,832	0,597
Case 14	1,5	7	49494	0,514	0,404	0,302
Case 15	2	7	52578	0,384	0,321	0,296
Case 16	1	4	29639	13,318	8,198	4,669
Case 17	1,5	4	46925	5,567	4,653	4,881
Case 18	2	4	50232	0,613	0,469	0,376

This set of simulations have been more troubling than the one with bonded contact. This is because some of the simulations did not converge at first, and they had to be redone several times changing some of the configuration values or the meshed elements.

In Figure 4.5 and Figure 4.6, the deformation of the clutch can be seen. In both cases the geometry and the loads are the same, the only difference is the connection between the two solids. The contact in Figure 4.5 is a bonded contact and the one in Figure 4.6 is a frictional contact. It can be seen that on the second case, relative movement between the inner and outer cage is possible. Otherwise, in the bonded case, both cages are deformed together.

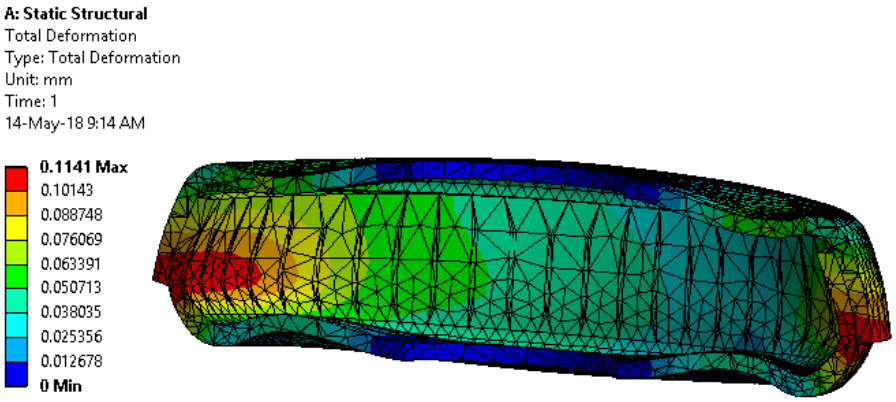

Figure 4.5: Section of the total deformation in case 2.

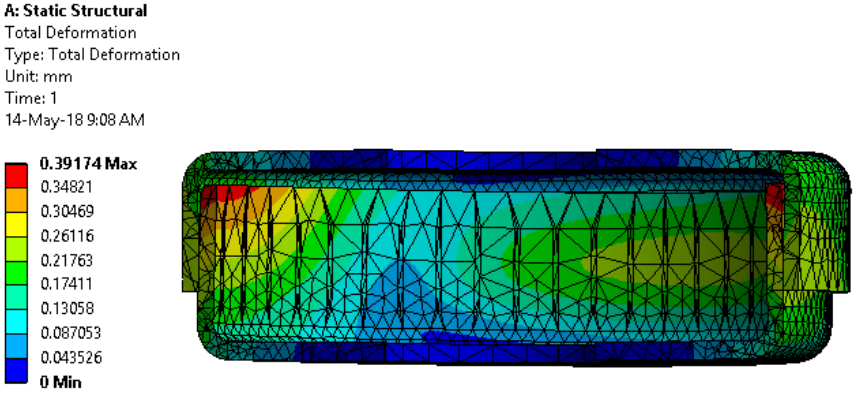

Figure 4.6: Section of the total deformation in case 11.

There are several specific cases in this set of simulations, case 16, case 17 and case 13. These cases have a larger deformation than the other cases do. For the case 16 and 17, this is because the outer cage is not holding the inner case when the loads are applied; the length of the outer cage is to short. Images of both cases can be seen in Figure 4.7 and Figure 4.8. In case 17, the outer case is not even deformed, that is because the part of the inner case where the pressure is applied slips down the outer cage, not creating any reaction on the outer case.

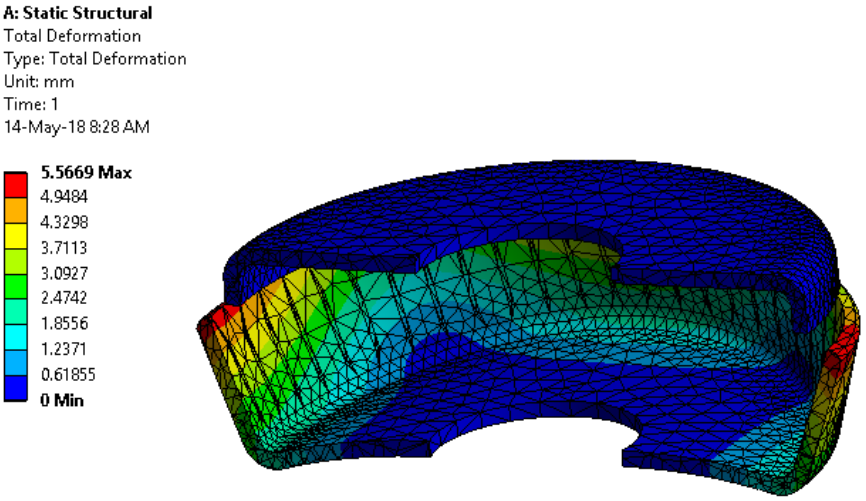

Figure 4.7: Section of the deformation in case 17.

On the other hand, in case 16, there is little deformation on the outer case. In this case, just one side of the inner case slips down the outer cage; the other side is still in contact with the outer part, creating this way a reaction that can deform it.

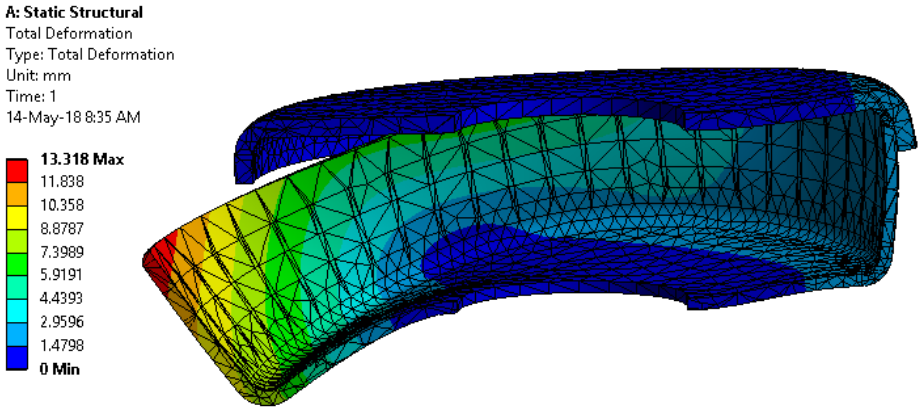

Figure 4.8: Section of the deformation in case 16.

Case 13 is one other simulation where the deformation is considerably. However, in this case, there is no slip from the inner cage; it is a regular deformation, as it can be seen in Figure 4.9. The maximum deformation is found on the top part of the inner cage, where the pressure is not applied, and it has a greater value than the other regular deformations because it has the thinnest wall.

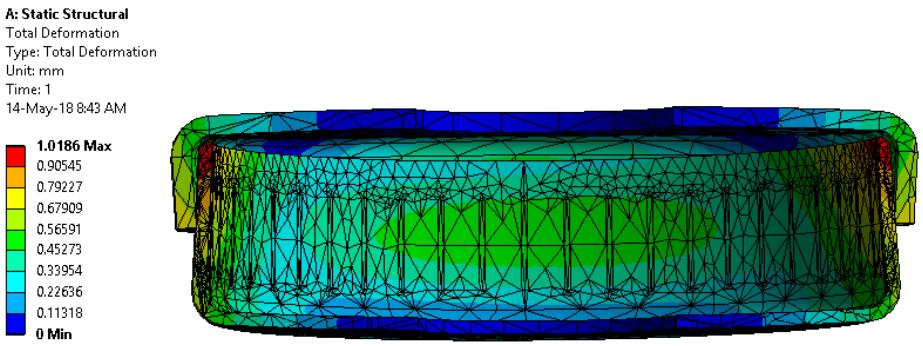

Figure 4.9: Section of the deformation in case 13.

In order to compare the values of the simulations the graphic in Figure 4.10 was made. In the graphic, the values of cases 16 and 17 were not taken into account. It has been decided to neglect those values because they are far from the mean, and it is already known what happens in those cases. As it can be seen on the graph, the simulation of case 12 (thickness = 2 mm and length = 10 mm) has a strange behaviour. It has more deformation than cases 15 and 11, and it should have less deformation due to the greater stiffness case 12 has compared to cases 15 and 11.

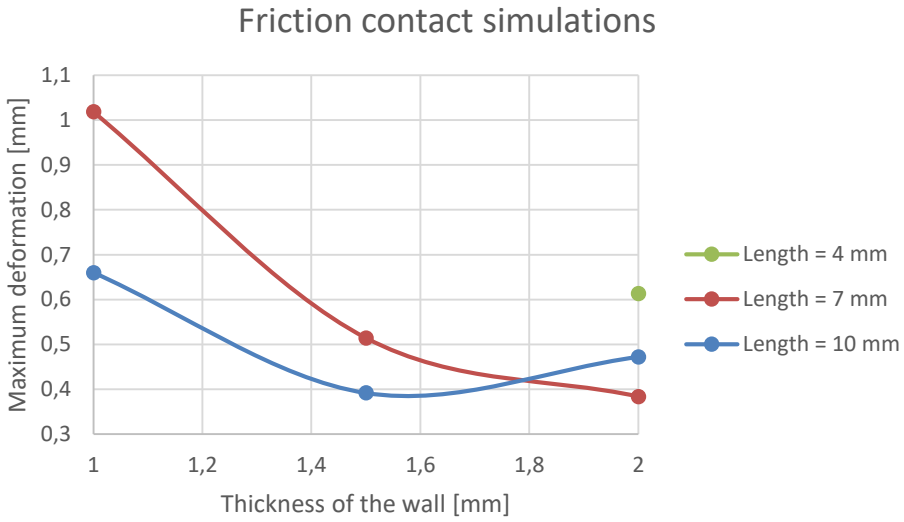

Figure 4.10: Frictional contact simulation results.

As it can be seen by comparing the values of Table 4.2 and Table 4.3, the results are quite different. Because of that difference, it is decided to continue only with the more realistic simulation, the frictional simulation. Because the deformation values are higher than the acceptable deformation of 0,1 mm, new simulations will be done. For these new set of simulations, the outer case with length of 4 mm will not be used, due to the problems it has entailed at converging the simulation and the poor behaviour they showed.

The next simulations that are done will only use the outer cage with a length of 7 mm and 10 mm, as it has been said before. The thickness of the inner cage will be increased until 5 mm, by increasing each step 0,5 mm, the results can be seen in Table 4.4. The deformation values, as it can be seen, are higher than the acceptable deformation for the clutch. Due to this, new simulations will be made again.

Table 4.4: Deformation values for the second set of simulations.

	Thickness [mm]	Length [mm]	Nodes	Max, Deformation [mm]	Max, Y deformation [mm]	Max, Z deformation [mm]
Case 19	2,5	10	55887	0,217	0,179	0,139
Case 20	3	10	57023	0,220	0,174	0,160
Case 21	3,5	10	60926	0,151	0,125	0,115
Case 22	4	10	66856	0,137	0,110	0,110
Case 23	4,5	10	67707	0,127	0,099	0,106
Case 24	5	10	69495	0,126	0,096	0,108
Case 25	2,5	7	56141	0,272	0,218	0,218
Case 26	3	7	55865	0,239	0,182	0,204
Case 27	3,5	7	59568	0,208	0,145	0,179
Case 28	4	7	65561	0,194	0,129	0,171
Case 29	4,5	7	67578	0,183	0,111	0,160
Case 30	5	7	69114	0,179	0,114	0,161

More simulations will be done until the deformation is inferior than the accepted tolerance value. For that purpose, the focus will be lay on the outer cage with the 10 mm length, whose deformation is closer to the accepted values. The results for these new simulations can be seen in Table 4.5. With a thickness of 6 mm the maximum deformation of the clutch is less than 0,1 mm. Therefore, the case 32 would be an acceptable design that meets the requirements.

Table 4.5: Deformation values for the third set of simulations.

	Thickness [mm]	Length [mm]	Nodes	Max. Deformation [mm]	Max. Y deformation [mm]	Max. Z deformation [mm]
Case 31	5,5	10	72960	0,106	0,083	0,097
Case 32	6	10	74908	0,098	0,075	0,093

Using the case 32 would mean being conservative, because the deformation that has been checked for the whole time is the one from the entire cage, the inner and the outer part. However, if the focus would lay only on the inner part, the weight of the cage could be reduced by choosing a lighter design. This design could be even lighter if the surface where the deformation is checked was only the sprag area. In Figure 4.11, both areas studied are shown.

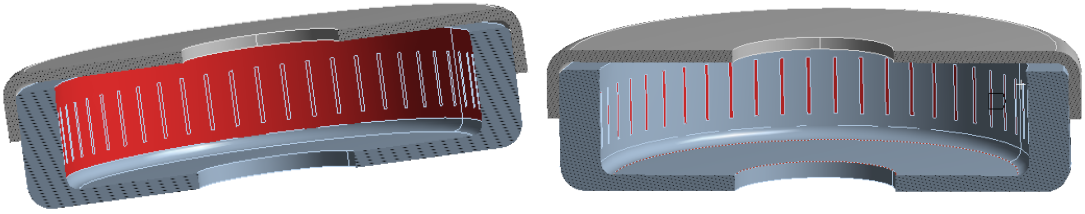

Figure 4.11: Inner surface (left) and sprag surface (right) for the deformation simulation.

In the Table 4.6, the deformation values of the previous simulations are showed. There are only the cases worth studying. That is why only seven cases are shown. Cases 29 and 30 were revised just in case their deformation value was below 0,1 mm, those are the only cases with a wall length of 7 mm. Cases 22, 23 and 24 have a deformation of the inner surface greater than 0,1 mm, therefore they will not be appropriate designs.

The only two cases that have a deformation below the tolerance accepted are cases 31 and 32. These are considered as good results, because most of the commercial sprag clutches have a thickness of the wall near 5 mm.

Table 4.6: Deformation values of the inner surface and the sprag surface.

	Thickness [mm]	Length [mm]	Max. deformation of the inner surface [mm]	Max. deformation of the sprag surface [mm]
Case 22	4	10	0,124	0,106
Case 23	4,5	10	0,131	0,097
Case 24	5	10	0,111	0,096
Case 29	4,5	7	0,132	0,122
Case 30	5	7	0,129	0,114
Case 31	5,5	10	0,093	0,084
Case 32	6	10	0,088	0,079

To have a better look on the results, some of the cases studied have been simulated again with the same loads but with some refinement on its mesh. These cases that have been studied in more detail are case 31 and 32, because they are the only cases that have values below 0,1 mm of deformation. As long as the interest is set on the maximum deformation of the inner part of the clutch, only the values of maximum deformation of the whole clutch and the values of maximum deformation of the inner surface of the clutch are shown. Those values can be seen in Table 4.7

Table 4.7: Deformation values of the mesh refined designs.

	Nodes	Max. Deformation [mm]	Max. deformation of the inner surface [mm]
Case 31	416868	0,106	0,094
Case 32	393820	0,098	0,089

If the values of the refined and not refined simulations are compared, it can be said that there is not much difference between those values. In both cases, the refined model gives a result of 0,001 mm more on the deformation of the inner surface. Therefore, the values of the first simulation were good enough to be accepted.

Once the values of deformation have been determined, the focus can lay on the stress values of the clutch. For this purpose, only the cases that have a deformation below 0,1 mm will be studied, therefore, the cases studied will be cases 31 and 32. In Table 4.8, the values of the stress of both cases 31 and 32 with the refined and not refined mesh can be seen.

Table 4.8: Stress values for cases 31 and 32.

	Maximum principal stress [MPa]	Maximum Equivalent stress (Von Mises) [MPa]
Case 31 (no-refined)	585,03	503,75
Case 31 (refined)	584,74	524,19
Case 32 (no-refined)	543,78	470,85
Case 32 (refined)	543,70	507,42

In this case, there is more difference between the values of the refined mesh than with the no-refined mesh, however, the difference of values is not as important as the location of the maximum values. In Figure 4.12 and Figure 4.13, the location of the maximum equivalent stress values can be seen for the case 31. As it can be seen, in the non-refined case, the maximum equivalent stress is located on the outer cage, whereas for the refined case, it is found on the inner cage, where the load is applied.

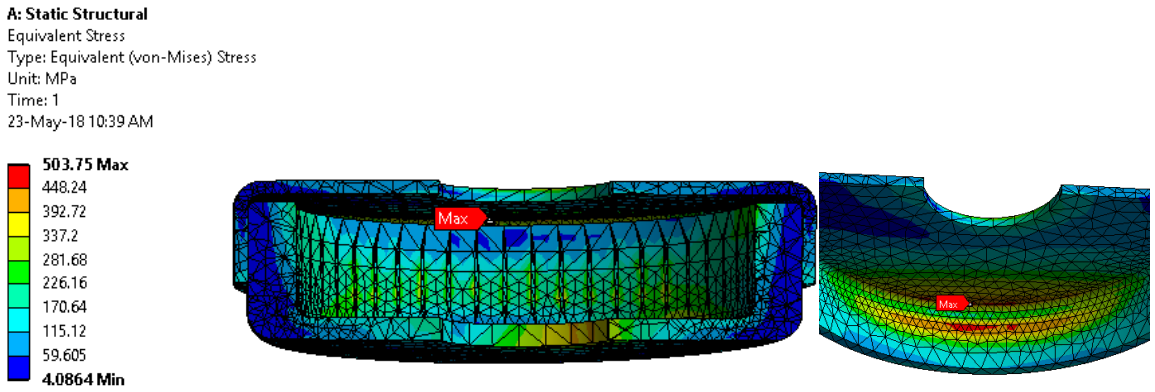

Figure 4.12: Equivalent stress value for non-refined case 31.

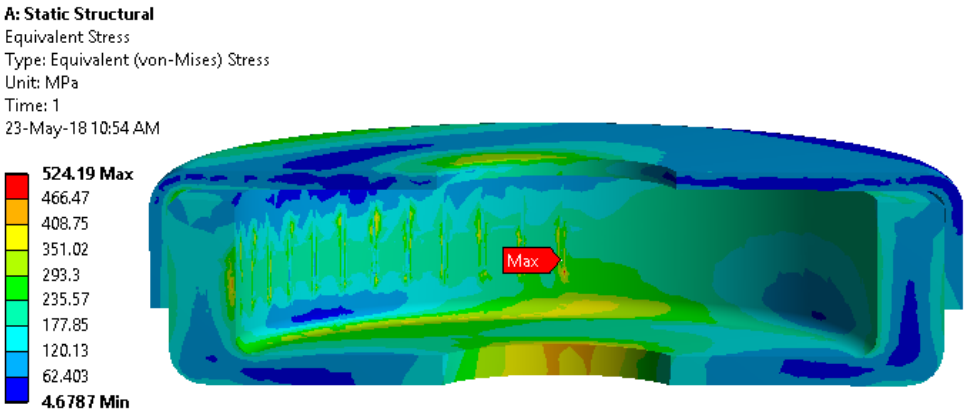

Figure 4.13: Equivalent stress values for refined case 31.

In Figure 4.14 and Figure 4.15, the values of equivalent stress for the non-refined mesh and the refined one of case 32 can be seen. Like in case 31, the maximum equivalent stress value for the non-refined case is found on the outer cage, and for the refined case, the maximum equivalent stress value is found on the inner cage.

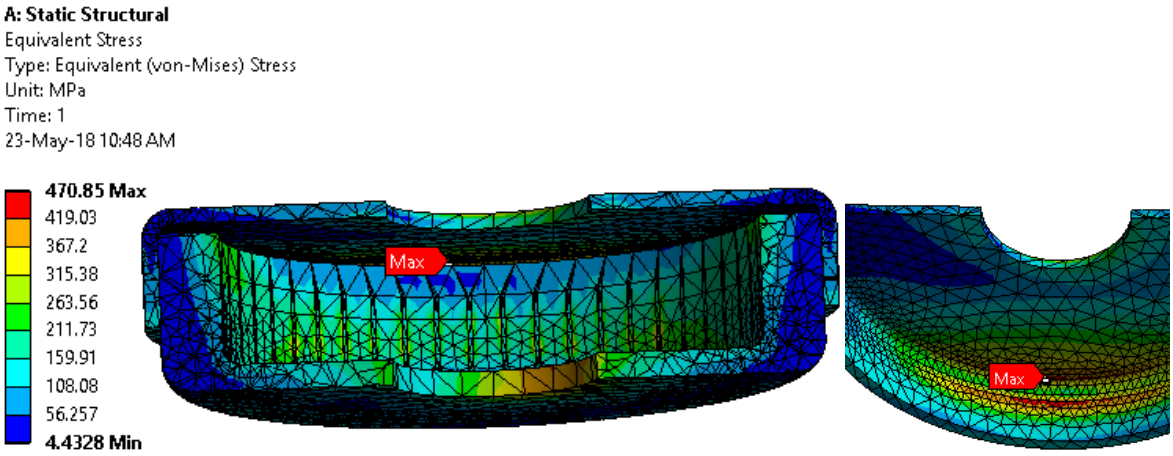

Figure 4.14: Equivalent stress values for non-refined case 32.

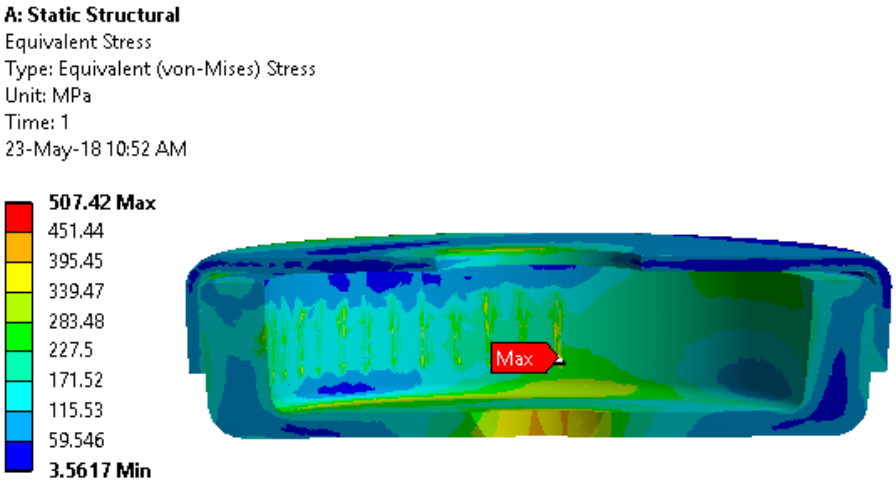

Figure 4.15: Equivalent stress values for refined case 32.

Just to be sure that the material will hold the loads of the clutch, the material yield strength should be over 530 MPa for case 31, and over 515 MPa for case 32. The limit values have been chosen a bit higher than the maximum value resulted from the simulation in order to have a factor of safety. Therefore, a steel that could bear those stresses should be found.

The proposed design is case 31, which has a maximum deformation on the sprag zone of less than 0,1 mm, and a von Mises stress level around 530 MPa. The weight of the designed cage is 217,24 g, but to this weight the weight of the commercial part has to be added and it has a weight of 27,50 g, which gives a total weight of 244,74 g. For these stress levels, a proper material to bear them could be SSAB Domex 550MC, a structural steel that has a 550 MPa yield strength, therefore, above the maximum stress level that the clutch should be loaded with.

4.1.3 Alternative results

The simulations have been done with the same parameters as the simple-cage clutch set of simulation. Once the two cases explained before in chapter 3.1.3 have been simulated, a great difference between both cases can be observed; the inclined wall case has much less deformation. Because of that great difference, one other case for the tightened wall is studied. The sketch for this second design can be seen in Figure 4.16, as it can be seen the tightened wall is 2 mm larger than the previous case.

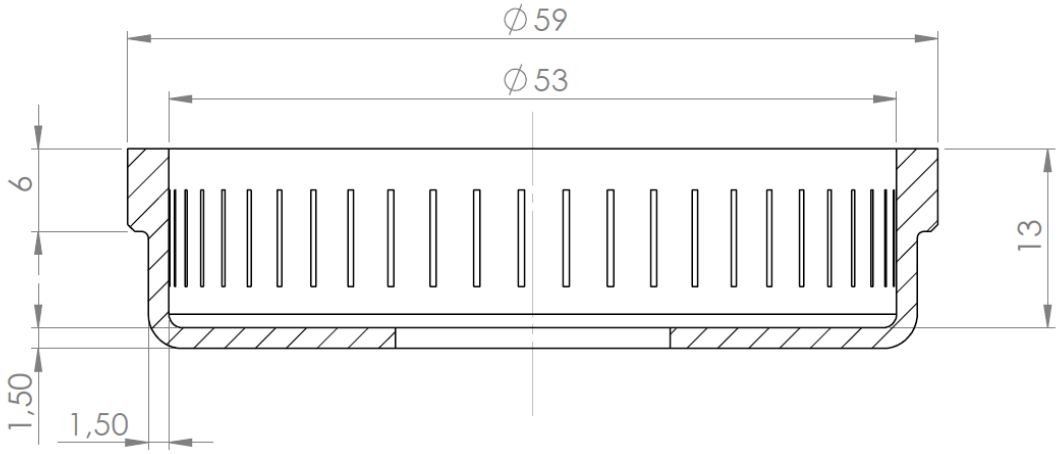

Figure 4.16: Sketch of the second design with the tightened wall.

In Table 4.9, the deformation values can be observed. As it has been said before, there is a great difference between the two different cases, tightened wall and inclined wall. After simulating the two cases of the tightened wall, they would be dismissed in comparison with the inclined wall case. The values obtained on the inclined wall case are more similar to the double-cage simulation results.

Table 4.9: Deformation values of the alternative simulations.

	Max. Deformation [mm]	Max. Y deformation [mm]	Max. Z deformation [mm]
Inclined wall	0,681	0,476	0,565
Tighter wall 1	2,799	2,242	2,211
Tighter wall 2	2,477	1,989	1,987

Therefore, if a choice between these two cases should be done, with no doubt the inclined wall would be the chosen design. However, it should be checked with the final design of the entire clutch and compare the price of fabrication between this design and a regular one, to see if the final price is competitive enough.

4.2 Ratchet and pawl clutch results

4.2.1 Outer part results

For the outer part simulation, the simulation has been set as a static structural simulation, with structural steel as a material. This material has a Young's Modulus of 200000 MPa and a Poisson's coefficient of 0,3. The mesh has been done with a quadratic element order. And the model used is a linear elasticity model.

As it has been stated before, two set of simulations have been done, the first one using three pawls and the second one using six pawls. The results of these two sets of simulations can be seen in the Table 4.10. The results as it can be seen are much lower compared to the Young's modulus, 200000 MPa. However, for regular structural steel, an acceptable value of yield strength is around 300 MPa.

Table 4.10: Deformation and stress values of the outer cage simulation.

	Max. deformation [mm]	Maximum principal stress [MPa]	Equivalent stress (Von Mises) [MPa]
3 pawls	0,065	800,47	651,43
6 pawls	0,048	382,1	331,97

In Figure 4.17 and Figure 4.18, the maximum equivalent stress is shown. Its maximum on both cases is located at the edge of the ratchet teeth where the load is applied. It was the expected spot where the maximum stress would appear, because edges and corners are zones where tension concentration appears.

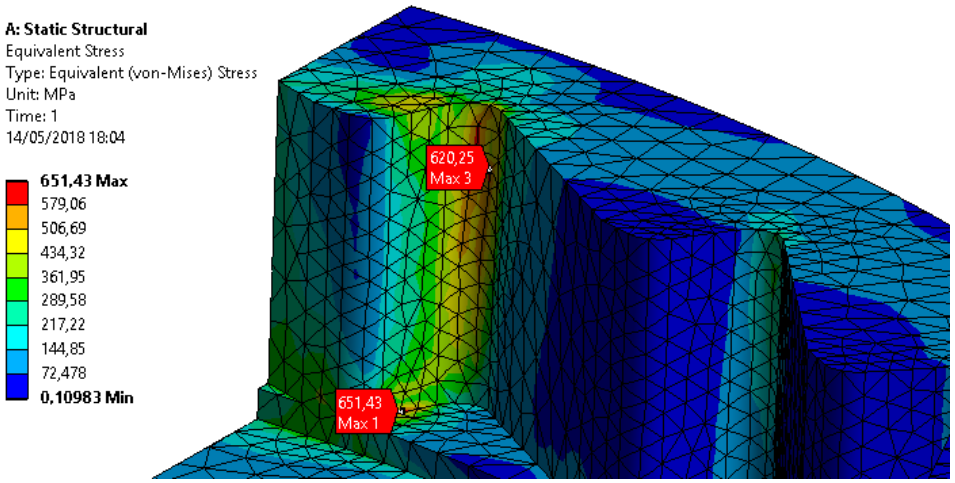

Figure 4.17: Maximum equivalent stress for the 3-pawl simulation.

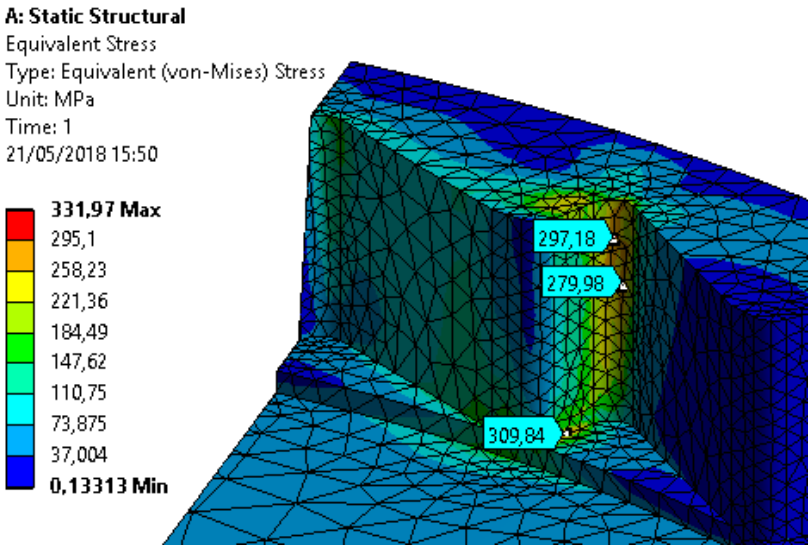

Figure 4.18: Maximum equivalent stress for the 6-pawl simulation.

Using a high quality steel for the whole clutch would be expensive, because of that it is thought of using a 6-pawls clutch instead of a 3-pawls one. Before taking a further decision, a new simulation will be done on the 6-pawls clutch. This time the mesh will be refined in order to verify the results obtained before. In Table 4.11,the values of this new simulation can be seen. The maximum deformation value is similar in both cases. However, the Von Mises stress is much higher, as it can be seen in Figure 4.19; it is due to a stress concentration point. The values around that point are inferior, therefore, that point can be neglected and consider the maximum von Mises stress as 340,27 MPa. This value is much closer to the non-refined simulation.

Table 4.11: Deformation and stress values for the refined outer 6-pawls simulation.

	Max. Deformation [mm]	Maximum principal stress [MPa]	Equivalent stress (Von Mises) [MPa]
6-pawls	0,0479	575,19	443,77

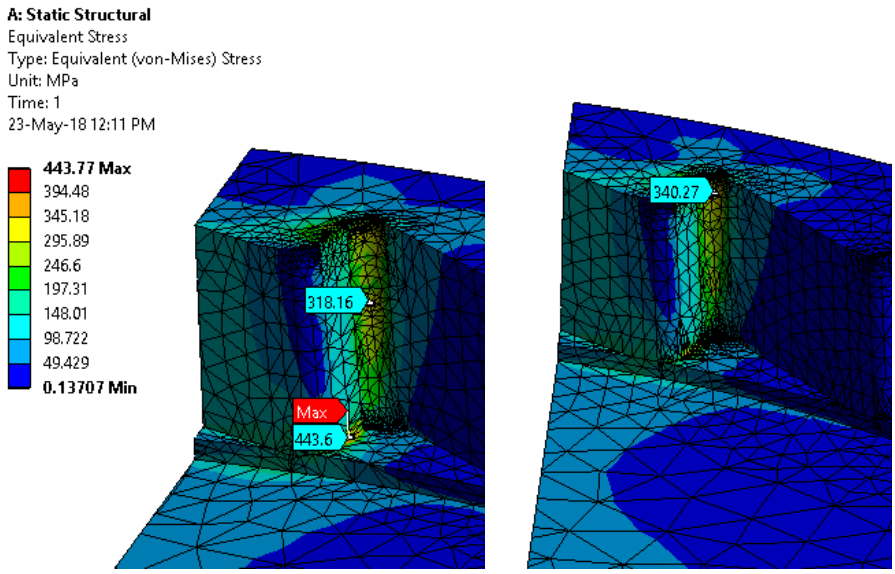

Figure 4.19: Equivalent stress values of the refined 6-pawl simulation.

With this value of 340,27 MPa, the outer cage should be made of steel that could bear the Von Mises equivalent stress. Therefore, steel S 355 [18] that has a yield strength of 355 MPa should be chosen for the outer part. However, the material decision will be done once the simulation of the whole clutch is made.

4.2.2 Inner part results

The simulations that have been made in the inner part result have the same properties as the simulations of the outer part. However, as the simulation of the complete inner has different elements, their contact had to be simulated. Therefore, the contact between the hammers and the inner part has been set as a bonded contact.

The results of the different simulations can be observed in Table 4.12. There are some differences between the values of the simulations of the complete inner part and the hammer-only. These differences come from the increase of the stiffness while simulating the complete inner part; the inner part holds some of the stress, decreasing the load of the hammer.

Table 4.12: Deformation and stress values of the inner part simulations.

Number of pawls	Simulation	Maximum deformation [mm]	Maximum principal stress [MPa]	Equivalent stress (Von Mises) [MPa]
3 pawls	Complete inner part	0,265	2388,7	2042,7
	Hammer-only	0,187	3559,4	2985,8

6 pawls	Complete inner part	0,137	1222,5	1025,4
	Hammer-only	0,092	1779,7	1492,9

In Figure 4.20, Figure 4.21, Figure 4.22 and Figure 4.23, the equivalent stress on the different simulations can be seen. The 3-pawls and the 6-pawls simulations have a similar distribution of the stress. As it can be seen, on the simulation of the complete inner part, the maximum stress is located on the outer part of the hammer. On the other hand, when the hammer is simulated alone, the maximum stress is located on the inner part of the hammer. This difference might be because of the boundary conditions set on the hammer-only simulation. The boundary condition of cylindrical support could lead to higher stresses on the border of that condition.

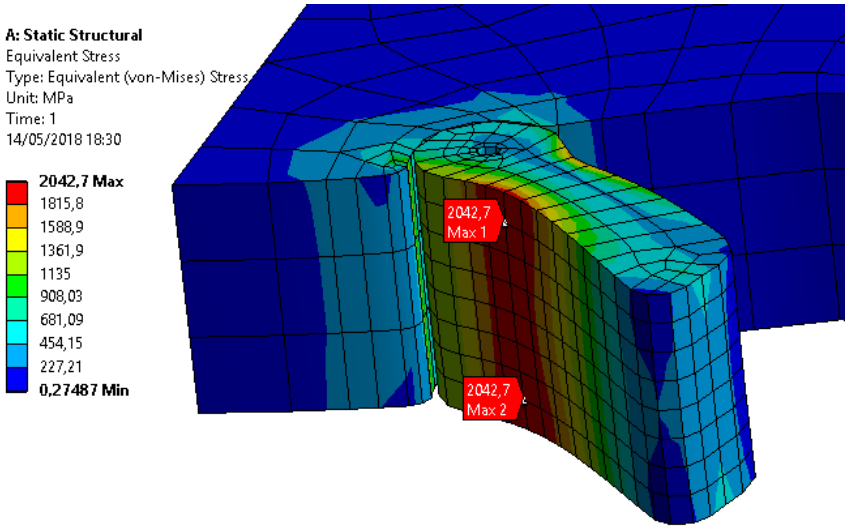

Figure 4.20: Equivalent stress for the 3-pawl complete inner part simulation.

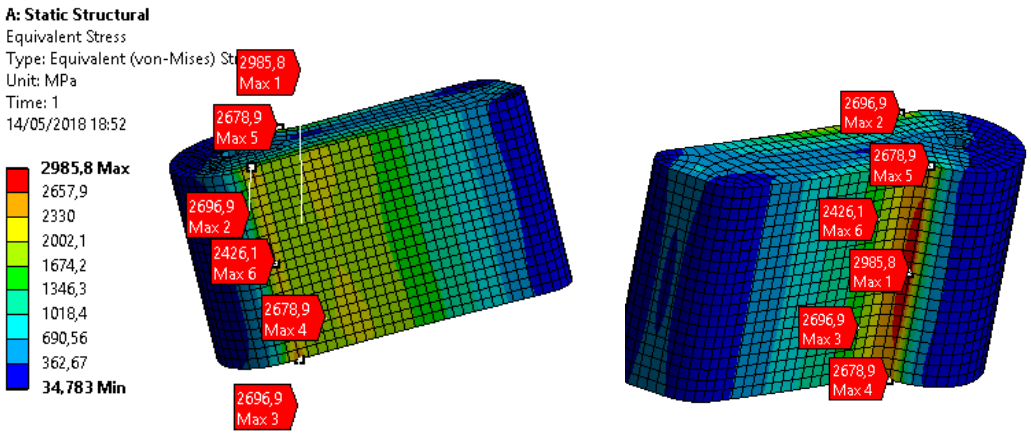

Figure 4.21: Equivalent stress for the 3-pawl hammer simulation.

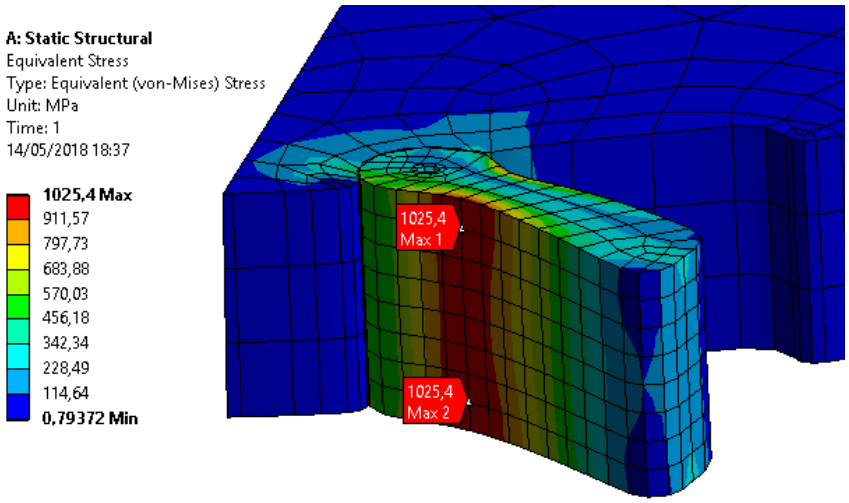

Figure 4.22: Equivalent stress for the 6-pawl complete inner part simulation.

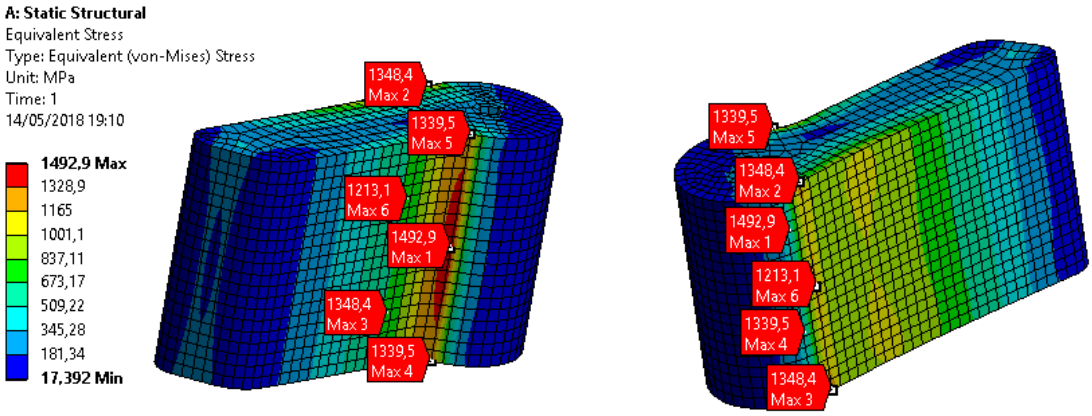

Figure 4.23: Equivalent stress for the 6-pawl hammer simulation.

The values of the 3-pawls simulation are too high; these stresses could not be borne by any competitive material. However, on the case of the 6-pawls, as the inner part of the clutch does not bear stresses over 320 MPa, the material proposed could be the same as the one proposed for the outer part of the clutch, S 335. However, before choosing a definitive material, new simulations with a refined mesh will be done for the 6-pawl clutch. This way the results obtained before will be checked.

In Table 4.13, the values of the refined simulation can be seen. As it happened on the outer cage case, the difference between the Von Mises stress of the refined and the not refined mesh is quite high. This big difference is due to the concentration of stress. This concentration of stress is found on the zone where the constraints change. Therefore, no conclusions can be extracted from these concentration points. Nevertheless, the hammers have to bear stresses levels of up to 1250 MPa. Therefore, a material that its yield strength is higher than this value should be found.

Table 4.13: Deformation and stress values for the refined inner 6-pawls simulation.

	Simulation	Maximum deformation [mm]	Maximum principal stress [MPa]	Equivalent stress (Von Mises) [MPa]
6 pawls	Complete inner part	0,146	1993,5	1724,3
	Hammer-only	0,094	1770,2	2790,9

As it can be seen in Figure 4.24, in the stress distribution there is a high concentration of stress where the boundary conditions change. If this stress concentration would not be taken into account, the maximum stress values would be around 1245 MPa.

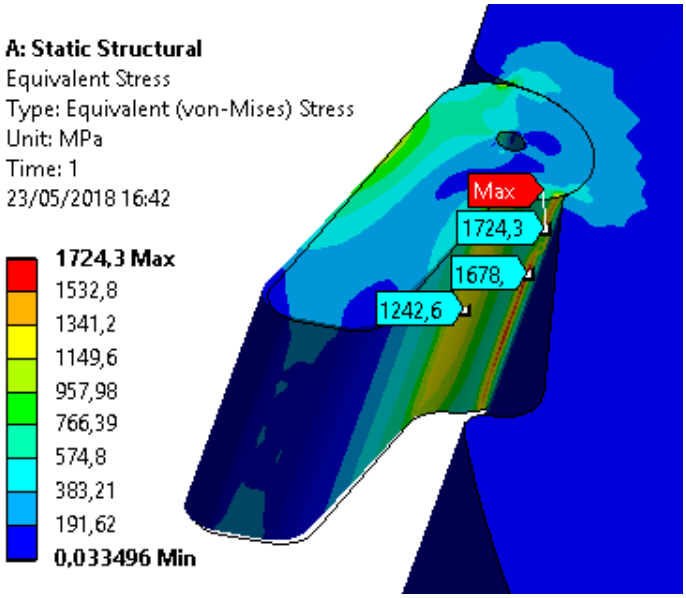

Figure 4.24: Equivalent stress values of the refined 6-pawls clutch.

This difference is easier to see in Figure 4.25, where the maximum stress value is 2790,9 MPa and around that point, the stress values are more or less 1400 MPa. Because of this great difference, in both cases, between the stress concentration and the stress values around that point, it can be said that it is not possible to extract proper information from this simulation, apart from getting an idea of the stress values that the hammer is receiving. In comparison, the non-refined simulation gives results more accurate, because there are no such great concentration stresses.

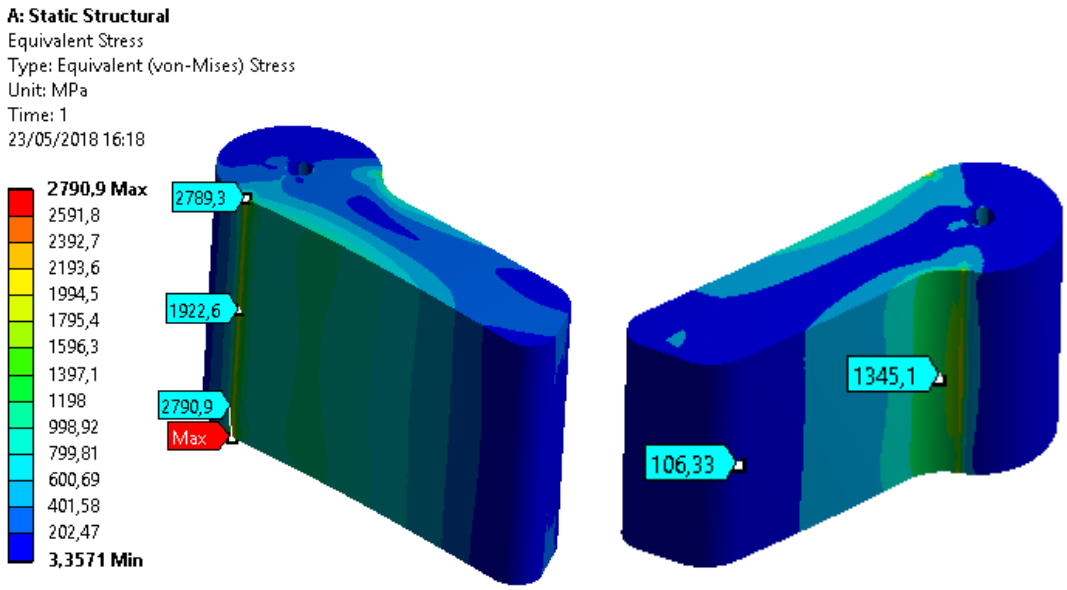

Figure 4.25: Equivalent stress values of the refined 6-pawls hammer simulation.

Therefore, to have results much more realistic, it has been decided to do a new simulation with the whole clutch, only the 6-pawls clutch will be simulated, because as it has been stated before, the 3-pawls clutch has to bear great stresses, and the result could not be economically competitive.

4.2.3 Complete part results

This new simulation will be done with the 6-pawls clutch, however, this time the simulation will be done in 2-D because the 3-D simulation did not converge. In this case the model used is a linear elasticity model also. The simulation thickness has been set to 5 mm and the 2-D behaviour has been set to stress. Two different sets of contact have been created to do this simulation. The first set of contact is the contact between the hammer and the inner part of the clutch, this contact is set to a bonded contact. The other set of contact is done between the hammers and the outer part, this contact is set to a frictional contact. In Figure 4.26, the contact connections can be seen, A connection is the bonded and B connection the frictional.

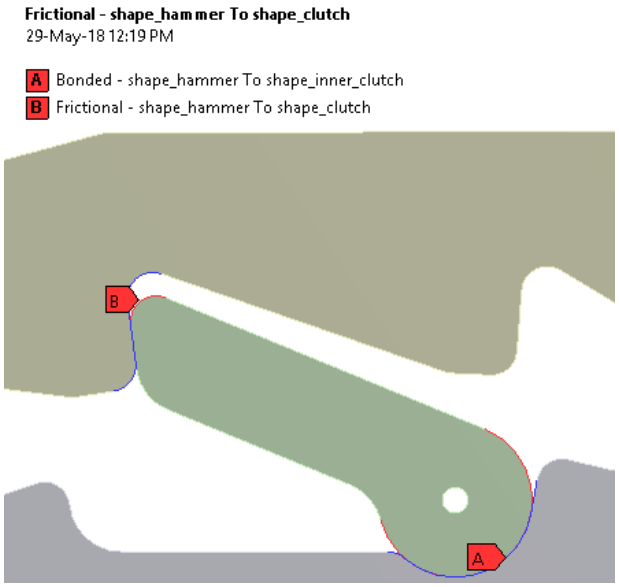

Figure 4.26: Contact connection on the complete.

The frictional contacts have almost the same definition as the frictional contact of the double-cage sprag clutch, and they have the next characteristics: a frictional coefficient of 0,15; an augmented Lagrange formulation; a detection method on Gauss point; a normal stiffness factor of 0,1 and the interface treatment as adjust to touch.

The load applied is the torque of 300 Nm; it is applied on the outer part of the outer hub. A part of the contact explained before, a fixed support has also been added on the inner part. The maximum results for the deformation and the von Mises stress are shown on Table 4.14. Each part has been studied separately to have values for all the parts used.

Table 4.14: Maximum deformation and equivalent stress on the complete simulation.

	Maximum deformation [mm]	Equivalent stress (Von Mises) [MPa]
Hammer	0,1239	1714
Inner part	0,0156	487,95
Outer part	0,1111	720,88

In order to study the deformation of the hammers, the deformation on the X and Y-axis will be studied. In Figure 4.27 and Figure 4.28, the deformation of the hammer on the X and Y-axis can be seen. As it can be see, the maximum deformation on the X-axis is around 0,082 mm and on the Y-axis is around 0,0955 mm. The problematic deformation is the suffered on the X-axis, because if the deformation is too high, the load may not be evenly distributed due to not all the hammers are working at the same time.

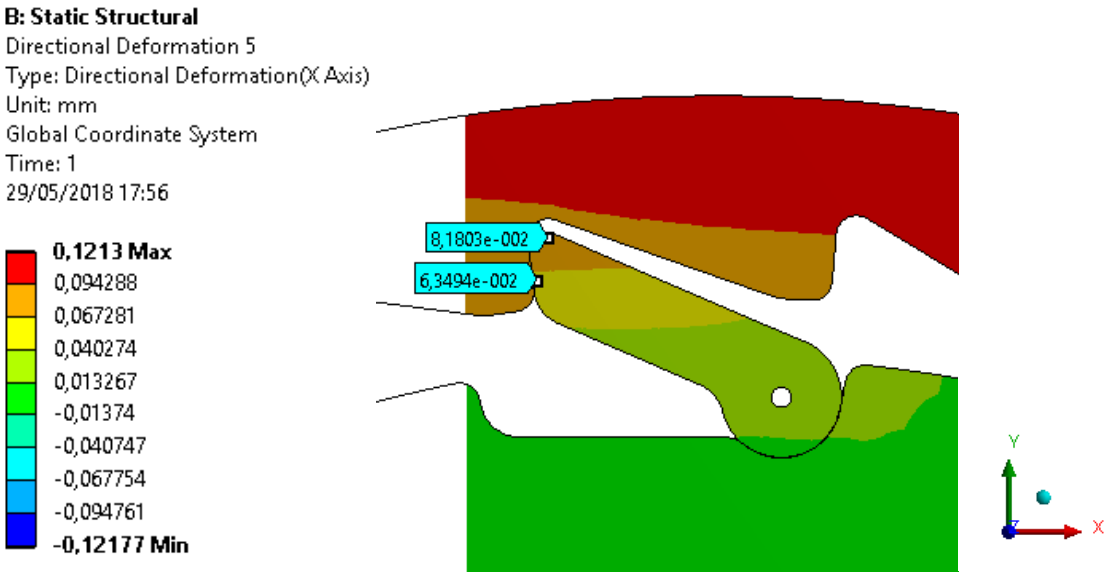

Figure 4.27: Deformation on the X-axis of the hammer.

Figure 4.28: Deformation on the Y-axis of the hammer.

On Figure 4.29, the total deformation of the same hammer can be seen. The maximum deformation value can be obtained with the Pythagoras' theorem, using the values of the maximum deformation on X and Y-axis.

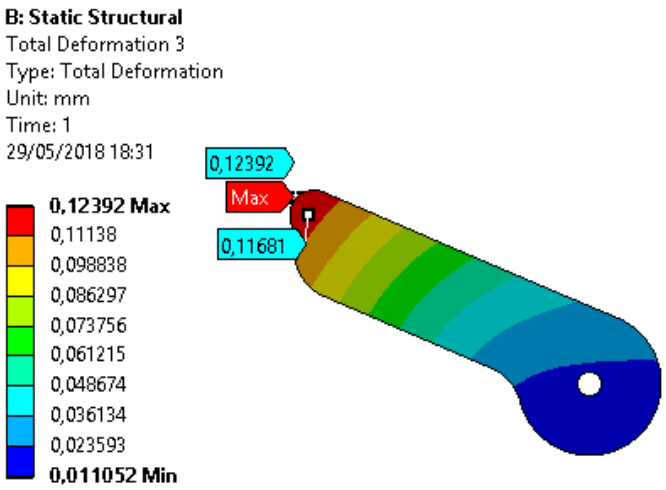

Figure 4.29: Total deformation distribution of the hammer.

As it can be seen in Figure 4.30, the von Mises stress on the hammer is concentrated on two lines. These lines of concentration are located where the bonded connection ends. Consequently, the maximum value of the von Mises stress cannot be accepted. Therefore, the maximum stress that appear on the hammers will be around 850 MPa, and it is found on the inner part of the hammer.

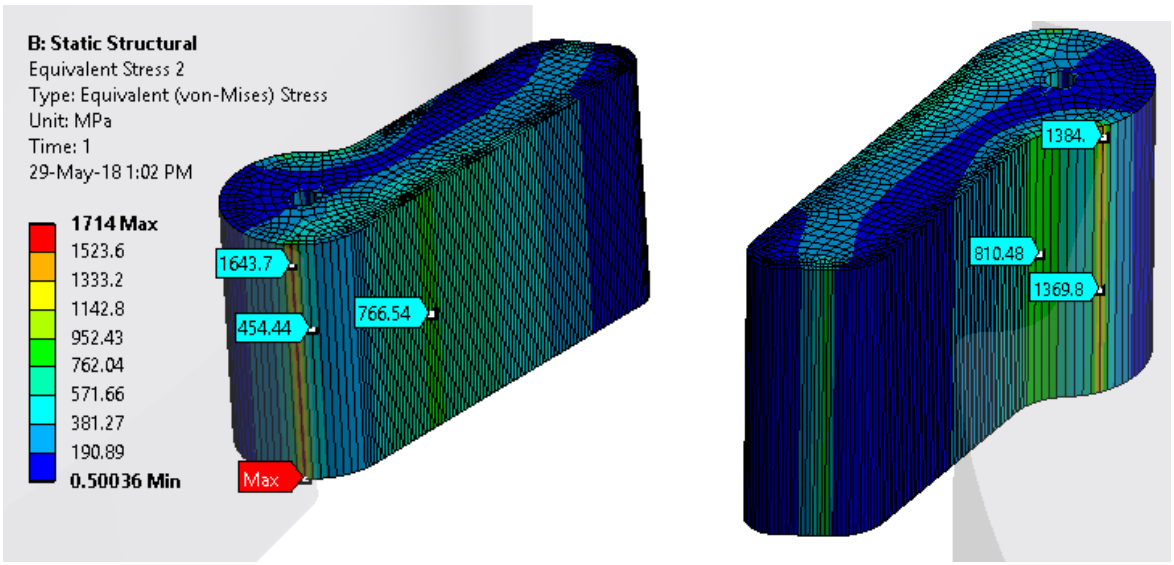

Figure 4.30: Von Mises stress concentration for the hammer part.

For the inner part, there is no need to look into detail for the deformation values, because they are much lower than the ones form the hammer and the outer part. Moreover, if they were high enough they would also affect to the hammer deformation.

As it can be seen in Figure 4.31, the distribution of the von Mises stress is concentrated on the housing of the hammer. The maximum value obtained is around 490 MPa, this value, unlike the hammer value, can be accepted because the values around this concentration point are more homogenous than the hammer ones.

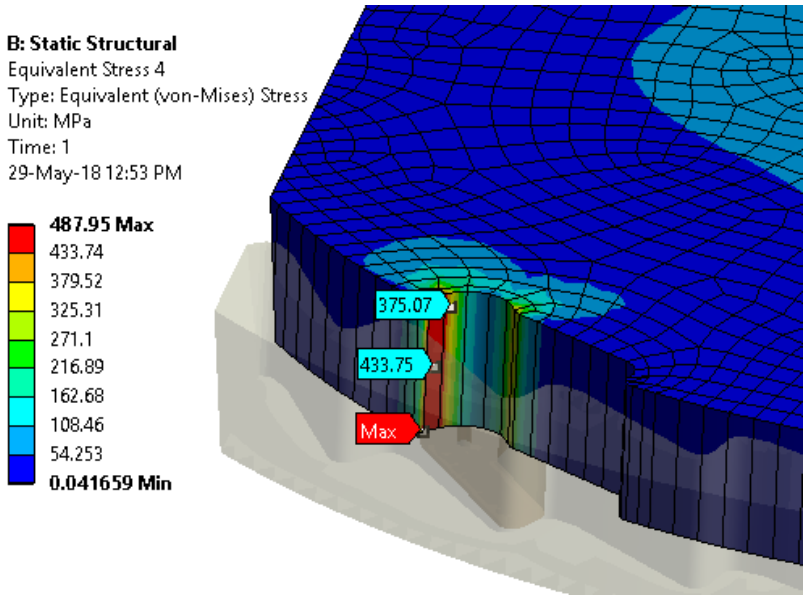

Figure 4.31: Von Mises stress concentration for the inner part.

The deformation of the outer part as the same problem as the deformation of the hammer, the problematic deformation is the one from the X-axis on the case studied. However, the deformation on the Y-axis will be checked. Both deformations can be seen in Figure 4.32 and Figure 4.33. As it can be seen, the deformation on the X-axis that will affect the torque transference is around 0,085 mm, and for the Y-axis is around 0,014 mm.

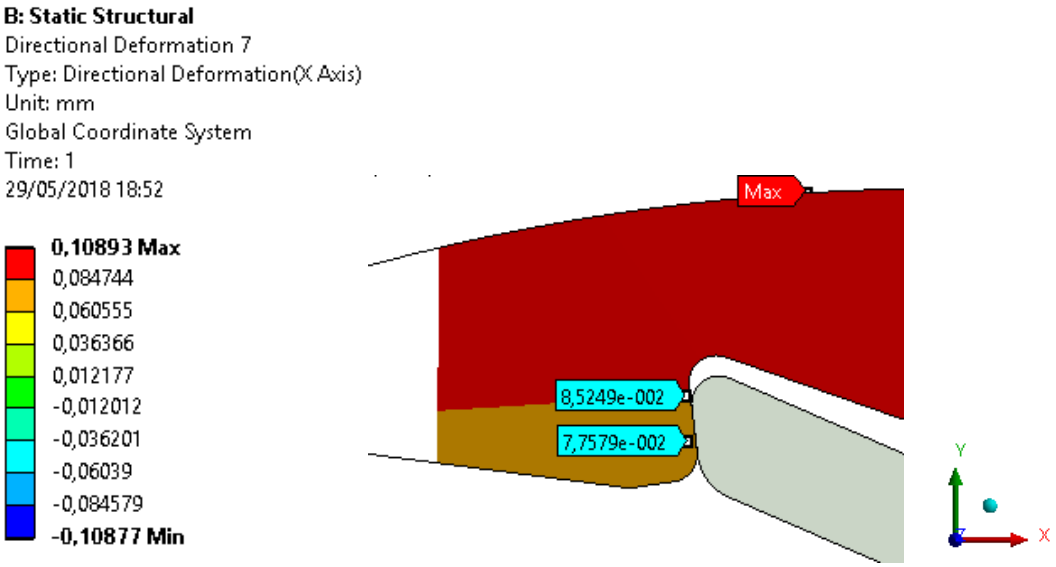

Figure 4.32: Deformation on the X-axis of the outer part.

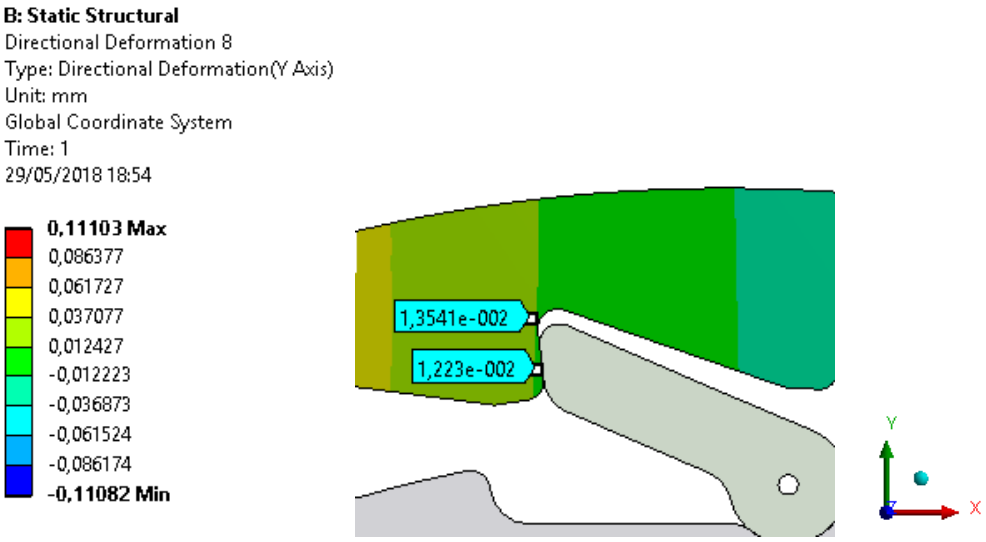

Figure 4.33: Deformation on the Y-axis of outer part.

The total deformation of the outer cage can be seen in Figure 4.34. As it happened on the hammer case, using the values of the X and Y deformations with the Pythagoras' theorem, the maximum value is gotten. In this case, on the hammer affected part is around 0,087 mm. After commenting the stress of this outer part, further comments about the deformation and the tolerances of the clutch will be made.

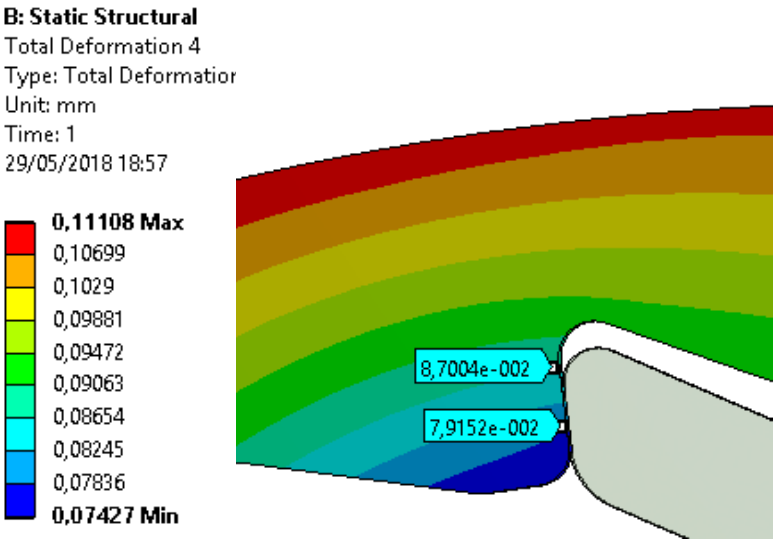

Figure 4.34: Total deformation distribution of the outer part.

The concentration stress of the outer part can be seen in Figure 4.35. As it can be seen, there is a high stress concentration where the hammer is in contact with the outer part. The maximum stress concentration is found there, and its values is around 720 MPa. On the inner corner of the outer part, more high concentration stresses can be found, however these have a lower value, and they around 500 MPa. In this case, the maximum stress is not as high as in the case of the hammer, and the stresses around the concentration point have values between 400 MPa and 500 MPa. Therefore, it can be said that 720 MPa might not be realistic, and the proposed maximum stress is 500 MPa, probably the outer part of the clutch will not get to this values. Therefore, the value of the 3-D simulation will be used.

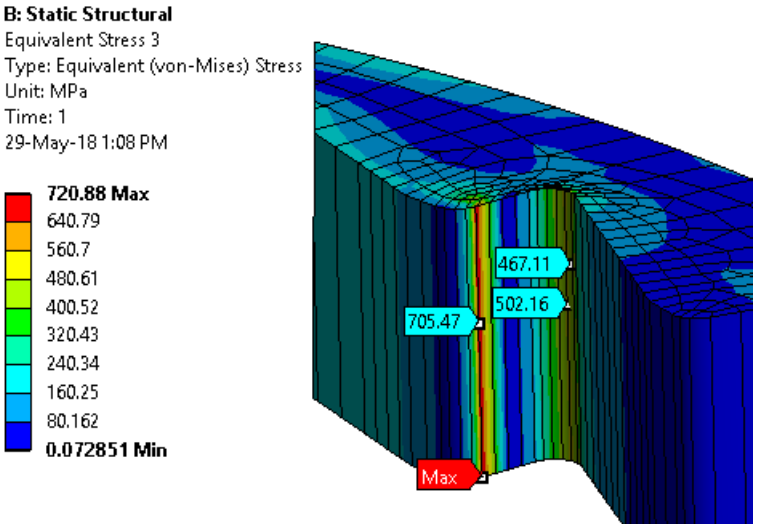

Figure 4.35: Von Mises stress concentration for the outer part.

One of the problems that can be found on the ratchet and pawl clutch is the deformation of the outer part and the hammers. If the deformation between those two parts is too high, the load will not be evenly distributed, because not all the hammers will be transferring the torque, consequently the ones that transmit the torque will have to bear higher stresses. The load to transfer would be the same, however instead of six pawls, maybe only three or four would be working.

As it has been seen during this chapter, the deformation on the X-axis of the hammer and the outer part of the clutch is around 0,08 mm. The X-axis will be the one studied because it is the one that affects the contact zone is the case studied.

The deformation obtained should be larger than the tolerances of fabrication. If this were the case, the contact of all the hammers with the outer part would be assured, therefore, the load would be distributed evenly and the simulation that has been made would be correct. If this were not the case, the simulation should be repeated with less hammers working. As it has been seen on the 3-pawl simulation, the stresses are much higher when only three of the hammers are working. This would mean that the materials proposed would not be accepted, and new materials with higher mechanical properties should be used.

Consequently, the tolerances of the outer part and the hammer have to be tight. The hammer part is apparently easier to produce than the outer part. Therefore, the tolerances of this part could be tighter than the ones from the outer part. It is supposed that the tolerance of the hammers could be around ± 0,01 mm and have a competitive price.

The tolerance of the outer part should be around ± 0,03 mm in order to fulfil the tolerances requirement and have them below 0,08 mm. As this part has a more complex shape, the price of its fabrication will be higher, a proper process of fabrication has to be searched, in order to have a competitive price for the clutch.

4.3 Comparison between the sprag and the ratchet and pawl clutch

Now that the simulations have been done and commented, it is time to do a summary of the clutches studied. On the Table 4.15, the main characteristics for each clutch can be seen. For the sprag clutch, the values used are the ones obtained on the refined simulation for the case 31. On the other hand, for the ratchet and pawl clutch, as there have been different simulations, the maximum stress values have been obtained from the different simulations, because the simulation values are varying for the different cases studied. Firstly, for the hammer, the values have been obtained from the 3-D simulation of the complete inner part. For the inner part, the value has been obtained from the maximum value of the 2-D simulation. Finally, for the outer part, the value has been obtained from the refined model 3-D simulation, because in comparison with the non-refined 3-D model.

Table 4.15: Main characteristics of the clutches studied.

	Sprag clutch	Ratchet and pawl	
Weight [g]	217,23		256,04
Maximum stress [MPa]	524,19	Hammer	1025,40
		Inner part	487,95
		Outer part	340,27

The proposed materials for each clutch part can be seen in Table 4.16. The values of the yield strength are, of course, above the maximum von Mises stress. The values of the material have been taken from the datasheet of each material [19]. Using these materials, would let both of the clutches to work correctly because there will not be plastic deformation. That would lead to permanent deformation of the parts, and after some working cycles it could lead to the breakdown of some of the parts, which, obviously, will became in gret damage for the clutch.

Table 4.16: Materials chosen for each clutch part.

	Material	Yield strength [MPa]	Tensile strength [MPa]
Sprag clutch	SSAB Domex 550MC	550	600-760
Ratchet and pawl: Hammer	Strenx 1100	1100	1250-1550
Ratchet and pawl: Inner part	SSAB Domex 500MC	500	550-700
Ratchet an pawl: Outer part	SSAB Domex 355MC	355	430-550

The sprag clutch has the deformation limitation of 0,1 mm, this limitation could be increased by changing the shape of the sprag as it has been explained at chapter 3.1, however, as a commercial sprag clutch should be used in order to keep a competitive price, the shape of the sprag cannot be changed. Therefore, the sprag clutch that would be used is case 31, which has a weight of 217,23 g.

On the other hand, the ratchet and pawl clutch used would be the design with six pawls, that weights 256,04 g. However, as this clutch has no commercial elements, it is possible to try to reduce the diameter of the clutch and therefore make it lighter.

Both clutches offer a good solution for letting the system work in a freewheeling position. However, the sprag clutch has the assembly problems that have been mentioned, and the limitation of the clutch deformation as inconvenient. On the other hand, the ratchet and pawl has the fabrication tolerances problem mentioned before, that can increase the price of the mechanism.

Moreover, one of the perks of using the sprag clutch in front of the ratchet and pawl, is that it is silent. However, this will not affect a lot to the person using the bicycle because there is another clutch in the electric bicycle, the one that is used in conventional bicycles also, which is a ratchet and pawl clutch. Therefore, the cyclist is already used to the sound of the clutch. In addition, the bicycle is meant to be used on the outside, where the sound of the clutch will be mixed with the environment.

5 Conclusions

Once all simulations have been done, some conclusions can be extracted after comparing both kind of clutches.

1) The obtained results indicate a similar behaviour between the two studied clutches. However, it would be more recommended to use the ratchet and pawl clutch, because if the tolerances proposed can be obtained, there should be no problem for the clutch to work properly. Nevertheless, for the sprag clutch, if there were any overload, the deformation would be higher than the allowed and the mechanism could be blocked.
2) As it has been demonstrated, the geometry of the sprags can be modified in order to improve the behaviour of this clutch. If their geometry is modified, the sprag clutch would accept a higher deformation than 0,01 mm, which will help to improve the clutch operation.
3) It is important to fulfil the tolerances parameters for the ratchet and pawl clutch in order to have an evenly distributed load on the hammers.

In this thesis a decision tree for choosing the right freewheel clutch has been done. After the first theoretical part, a description of the two clutches used during the prototypes and the definition of the ones used in the simulation has been done. After simulating the designed clutches, the conclusions above could be extracted.

Recommendations for future research

In addition to this study, some steps should be done in the future:

- Compare the fabrication systems in order to get the best relation between price and quality.
- Test real prototypes to verify the results obtained during the simulations are acceptable.
- Improve the ratchet and pawl design in order to be less sensitive to the deformation received.

6 Bibliography

[1] *Element FE 448 Z2*. In: GMN. Available at: https://www.gmnbt.com/sc-fe-448-z2-insert-element.htm, Retrieved: 15 March 2018.

[2] *Element FE 453 M*. In: GMN. Available at: https://www.gmnbt.com/sc-fe-453-m-insert-element.htm, Retrieved: 15 March 2018.

[3] J. H. Bickford, *12 Ways to go 1 Way*, Machine Design, Vol. 40, No. 18, 1968.

[4] W. C. Orthwein, *Clutches and Brakes Design and Selection*, Marcel Dekker, Inc., New York, 1986.

[5] Altra Industrial Motion: Overrunning Clutches Application Manual [Altra Industrial Motion, Inc ltd Headquarters, USA]. Altra Industrial Motion, USA, 2014.

[6] C. F. Wiebusch, *The Spring Clutch*, Journal of Applied Mechanics, Vol. 6, 1939.

[7] *M-Series Magnetic clutch*. In: Tiny-clutch. Available at: http://www.tinyclutch.com/magnetic-clutches.htm Retrieved: 20 March 2018.

[8] Ringspann: Freewheels [Ringspann, Inc ltd Headquarters, Germany]. Ringspann, Germany, 2017.

[9] Cross-Morse: Freewheel [Cross-Morse, Inc ltd Headquarters, United Kingdom]. Cross-Morse, United Kingdom, 2008.

[10] Xu, T. and Lowen, G., *A Mathematical Model of an Over-running Sprag Clutch*, Mechanism and Machine Theory, Vol. 29, No. 1, 1994.

[11] M. Neale, *Tribology Handbook*, Butterworth Heinemann, Oxford, 1995.

[12] GMN, Sprag type Freewheel Clutches, [GMN, Inc. ltd Headquartes, Germany]. GMN, 2013.

[13] Tsubaki: CAM Clutch [Tsubaki, Inc ltd Headquarters, Japan]. Tsubaki, Japan 2016.

[14] Renold: Sprag Clutch [Renold, Inc ltd Headquarters, United Kingdom]. Renold, United Kingdom, 2011.

[15] C. Riba, *Mecanismes i màquines I: El frec en les màquines*, Edicions UPC, Barcelona, 1999.

[16] C. Huang, M. Liu and Y. Zaho, *An Analytical Model of Multiarc Sprag Clutch considering Geometry and Internal Interactioin during Engagement,* Shock & Vibration. 3/21/2017.

[17] Z. Liu, H. Yan and Y. Cao, *Design and analysis of logarithmic spiral type sprag one-way clutch*, Journal of Central South University, Vol. 22, No. 12, 2015.

[18] C. Riba, *Disseny de màquines IV: Selecció de materials 1*, Edicions UPC, Barcelona, 2005.

[19] *SSAB - High Strength Steel*. Available at: https://www.ssab.com, Retrieved: 28 May 2018.